Electrowinning of Zinc for the anode of Rechargeable Hybrid Aqueous Batteries (ReHABs)

by

Yan YU

A thesis
presented to the University of Waterloo
in fulfillment of the
thesis requirement for the degree of
Master of Applied Science
in
Chemical Engineering

Waterloo, Ontario, Canada, 2015

Author's Declaration

I hereby declare that I am the sole author of this thesis. This is a true copy of the thesis, including any required final revisions, as accepted by my examiners.

I understand that my thesis may be made electronically available to the public.

Abstract

A rechargeable hybrid aqueous battery (ReHAB) system has recently been developed by our research group. In order to improve the anode material, electrowinning technique has been introduced to produce four different types of Zn anodes with various combinations of additives Bi, In, thiourea and gelatin (labeled as BG#1, TG#1, ITG#1 and hBITG#1).

The resulting Zn anodes have been fully characterized for their electrochemical and battery performance. The results have been compared with commercial Zn.

X-ray diffraction (XRD) pattern results indicate that during the electrowinning Zn has been deposited preferably along certain crystal directions. From scanning electron microscopy (SEM) images on relatively low magnification, commercial Zn foil shows cutting marks which might be caused by the cutting process with the manufacturer. While all anodes prepared by the electrowinning show relatively uniform surfaces. On relatively higher magnifications, the morphology of BG#1 is flat hexagonal & non-porous, TG#1 is fine-grained & porous, ITG#1 has relatively medium grain size & porous, and hBITG#1 is coarse-grained & porous.

All anodes exhibit similar corrosion potentials and TG#1 performs the lowest corrosion current at 723.824 μA (per 1.1 cm^2), follow by ITG#1, commercial Zn, BG#1 and hBITG#1. It means that the anode TG#1 possesses the best corrosion resistance.

After 200 cycles for CC-CV protocol, batteries using commercial Zn anodes had capacity retention of 78.2%, yet batteries with BG#1, TG#1, ITG#1 and hBITG#1 anodes had 82.6%, 84.3%, 75.0%, and 71.9% capacity retention, respectively. While after 300 cycles, batteries with BG#1, TG#1, ITG#1 and hBITG#1 anodes had 73.2%, 77.2%, 66.2%, and 59.8% capacity retention respectively, yet batteries using commercial Zn anodes were all dead between 220-270 cycles. The results indicate that the TG#1 is the best choice for preparing anode material for the ReHAB. And all electrowinning Zn anodes are relatively stable compare to commercial Zn. The polarization resistances of batteries measured by

electrochemical impedance spectroscopy (EIS) for all kinds of Zn anodes after cycles didn't have exactly the same trend. The battery with the BG#1 anode has smallest polarization resistance which means it consumes the minimum energy during charge-discharge process, followed by the hBITG#1, the commercial Zn, the ITG#1 and the TG#1.

At room temperature (25 ℃), float charge current of commercial Zn and hBITG#1 at 2.1V have largest values meaning more side reactions happening in the batteries, followed by TG#1, BG#1 and ITG#1. At high temperature (60 ℃), the trend was the same. Elemental analysis results indicate that batteries with BG#1 anode has the most carbon on cathode material after both room temperature float charge (RTFC) and high temperature float charge (HTFC) tests. This suggests those with BG#1 anode are the most stable on cathode material with least structure collapse during float charge processes, followed by hBITG#1, TG#1, ITG#1 and commercial Zn.

Both BG#1 and TG#1 anodes show good overall performance. The advantages on battery performance of BG#1 anodes could be attributed to the uniform deposits, preferable crystal orientations and high corrosion resistance, and which of TG#1 anodes could be attributed to the porous and fine-grained deposits, preferable crystal orientations and high corrosion resistance.

Acknowledgements

First and foremost, I would like to express my greatest gratitude my parents and my family, without their supports I cannot happily study and live in Canada. Specially thank you my wife Jin SHI, you have brought a lovely miracle to our life and I really enjoy being a father.

I would like to thank my supervisor, professor Pu Chen, who guided me and provided good experimental conditions throughout the period of my master graduate degree program.

Besides, I would like to send my thanks to some members in the battery group: Dr. Xianwen WU, who helped me a lot on experimental design; Dr. Tuan Hoang, who dedicated on my thesis and paper revision. I would like to give special thanks to all the other researchers in professor's group, all my friends and working staffs in the university for the valuable friendship and support.

Last but not least, I would like to thank University of Waterloo to give me such an opportunity to broaden my knowledge and vision in Canada.

Dedication

This thesis is dedicated to my family, especially my little son David.

List of Figures

List of Tables

List of Abbreviations

ReHAB: Rechargeable hybrid aqueous battery

XRD: X-ray diffraction

EIS: Electrochemical impedance spectroscopy

RTFC: Room temperature float charge

HTFC: High temperature float charge

SEM: Scanning electron microscopy

PVDF: Polyvinylidene fluoride

NMP: 1-methyl-2-pyrrolidinone

KS6: KS6 graphite

CCCV: Constant current / constant voltage protocol

Nomenclature

F	Faraday's constant (96, 487C/mol)
I	Current (A)
j	Current density across electrode/electrolyte interface (A/m2)
R	Universal gas constant (8.314J/(mol·K))
t	Time (s)
T	Temperature (K)
η	Overpotential (V)
Ecorr	Corrosion potential (V)
i_a/i_c	Anodic/Cathodic current density (A/m2)
icorr	Corrosion current density (A/m2)
η_C	Coulombic efficiency

Table of Contents

Chapter 1

Introduction

1.1 Development of the battery

Battery, in electricity and electrochemistry, is any of a class of devices that convert chemical energy directly into electrical energy. Each cell contains a positive terminal, or cathode, and a negative terminal, or anode. Electrolytes allow ions to move between the electrodes and terminals, which allows current to flow out of the battery to perform work. [1] The anode is the negative electrode of a cell associated with oxidative chemical reactions that release electrons into the external circuit, while the cathode is the positive electrode of a cell associated with reductive chemical reactions that gain electrons from the external circuit on discharge process. The charge process carries the opposite way. An electrolyte is a material that provides pure ionic conductivity between the positive and negative electrodes of a cell. [2]

Batteries are divided into two general groups: ①primary batteries and ② secondary,

or storage, batteries. Primary batteries are designed to be used until the voltage is too low to operate a given device and are then discarded. Primary batteries are assembled in the charged state; discharge is the primary process during operation. [2] "Primary" batteries could produce current as soon as assembled, but once the active elements are consumed, they could not be electrically recharged. [3] A secondary battery is a cell or group of cells for the generation of electrical energy in which the cell, after being discharged, may be restored to its original charged condition by an electric current flowing in the direction opposite to the flow of current when the cell was discharged. Other terms for this type of battery are rechargeable battery or accumulator. As secondary batteries are usually assembled in the discharged state, they have to be charged first before they can undergo discharge in a secondary process.[2] Secondary batteries have many special design features, as well as particular materials for the electrodes, that permit them to be reconstituted (recharged). After partial or complete discharge, they can be recharged by the application of direct current (DC) voltage. While the original state is usually not restored completely, the loss per recharging cycling in commercial batteries is only a small fraction of 1 percent even under varied conditions. [4]

1.1.1 Early Batteries

The Italian physicist Alessandro Volta is generally credited with having developed the first operable battery. Following up on the earlier work of his compatriot Luigi Galvani, Volta performed a series of experiments on electrochemical phenomena during the 1790s. By about 1800 he had built his simple battery, which later came to be known as the “voltaic pile.” This device consisted of alternating zinc and silver disks separated by layers of paper or cloth soaked in a solution of either sodium hydroxide or brine. Experiments performed with the voltaic pile eventually led Michael Faraday to derive the quantitative laws of electrochemistry (in about 1834). These laws, which established the exact relationship between the quantity of electrode material and the amount of electric power desired, formed the fundamental of modern battery technology.

Various commercially significant primary cells were produced on the heels of Faraday's theoretical contribution. In 1836 John Frederic Daniell, a British chemist, introduced an improved form of electric cell consisting of copper and zinc in sulfuric acid. The Daniell cell, which consists of a copper pot filled with a copper sulfate solution, in which was immersed an unglazed earthenware container filled with sulfuric acid and a zinc electrode[3], was able to deliver sustained currents during continuous operation far more efficiently than Volta's device. Further advances were effected in 1839 by the British physicist William Robert Grove with his two-fluid primary cell consisting of amalgamated zinc immersed in dilute sulfuric acid, with a porous pot separating the sulfuric acid from a strong nitric acid solution containing a platinum cathode. The nitric acid served as an oxidizing agent, which prevented voltage loss resulting from an accumulation of hydrogen at the cathode. The German chemist Robert Wilhelm Bunsen substituted inexpensive carbon for platinum in Grove's cell and thereby helped promote its wide acceptance.

In 1859 Gaston Planté of France invented a lead-acid cell, the first practical storage battery and the forerunner of the modern automobile battery. Planté's device was able to produce a remarkably large current, but it remained a laboratory curiosity for nearly two decades.

French engineer Georges Leclanché's prototype of the zinc–manganese dioxide system paved the way for the development of the modern primary battery. The invention of alkaline electrolyte batteries (specifically, storage batteries of the nickel-cadmium and nickel-iron type) between 1895 and 1905 provided systems that could furnish much-improved cycle life for commercial application. The 1930s and '40s saw the development of the zinc–silver oxide and zinc–mercuric oxide alkaline batteries, systems that provided the highest energy yet known per unit weight and volume. Since the mid-20th century, advances in construction technology and the availability of new materials have given rise to smaller yet more powerful batteries suitable for use in a wide array of portable equipment. Perhaps most notable have been the entrance of lithium batteries into the commercial market and the development of nickel-hydrogen

and nickel–metal hydride cells for use in spacecraft, computers, cellular telephones, and other applications. [4]

1.1.2 Lithium-ion Battery

Traditional batteries have their defects, such as low energy density, high weight and large size, which rised up the requirement of high energy density battery— the Li-ion battery.

Research and development of the lithium-ion (Li-Ion) battery system began in the early 1980s at Asahi Chemicals. In order to meet the lightweight and high energy density requirements, in 1991 Japanese company Sony first commercialized lithium-ion battery, and it has been popularly used in our current portable electric devices since then.

The higher volumetric and gravimetric energy storage capability are key characteristics of the Li-Ion battery system compared to the conventional sealed nickel–cadmium (Ni–Cd), nickel-metal hydride (Ni-MH), and valve-regulated lead acid (VRLA) battery systems (Fig. 1.1). For a given cell size, larger values of Wh/l and Wh/kg translate into smaller and lighter cells. These characteristics became the enabling technology for the proliferation of portable battery-powered electronic devices, especially notebook computers and mobile phone applications. [5]

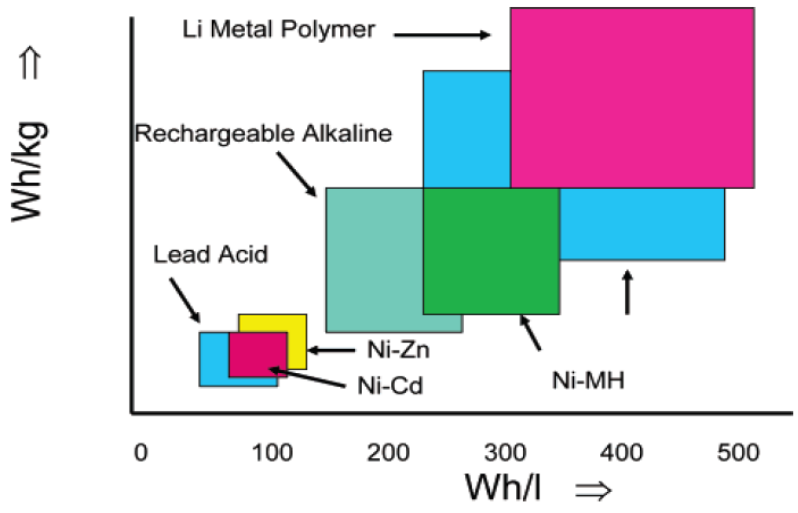

Figure 1.1: Energy storage capability of common rechargeable battery systems. [2]

Safety of the system has been a watchword for Li-ion batteries. They have the ability to self-destruct if abused. Manufacturers are careful to ensure that the cells are safe in normal operations. In addition, cell designs incorporate features such as devices that shut off current flow when an abuse condition arises. The United Nations [6] as well as the transportation agency in each country have requirements for testing to ensure a safe product for shipping.

Although research on decreasing the risk of a safety incident as well as the cost of battery producing have reached some remarkable achievements[7], there are still some issues and challenges facing rechargeable lithium batteries[8]. Table 1.1 shows the advantages and disadvantages of the Li-Ion rechargeable batteries.

Table 1.1 Advantages and disadvantages of Li-ion rechargeable cells

Advantages	Disadvantages
• Chemistry with the highest energy (Wh/g) and lightest weight (Wh/kg)	• Relatively expensive
• No memory effect	• Lightest weight
• Good cycle life	• Requires protection circuitry for safety and to prevent overcharge and overdischarge
• High energy efficiency	• Nominal 3-h charge
• Good high-rate capability	• Not tolerant of overcharge and overdischarge
	• Thermal runaway concerns
Added advantages and disadvantages of Li-Ion polymer/laminate cells	
• Flexible footprint	• Limited high rate capability
• Plasticized electrolyte	• More expensive
• Internal bonding of anode	• Poor low-temperature performance
• Cathode and separator	

1.1.3 Aqueous Battery

Due to the safety issues, such as flammability and toxicity, on lithium ion batteries, researches started to look back to “wet” batteries. In 1994, Dalhousie University professor Jeff Dahn first proposed the idea of the aqueous based lithium-ion battery [9]. He used $LiMn_2O_4$ and VO_2 as electrodes and 5M $LiNO_3$ solution as the electrolyte. Lithium batteries with aqueous electrolytes provided a nice solution to the traditional lithium-ion battery problem which based on organic electrolytes. After that, more research on different aqueous battery types followed [10-12].

1.1.4 Rechargeable Hybrid Aqueous Battery

A new aqueous rechargeable battery combining an intercalation cathode with a metal (first order electrode) anode has been invented by professor Pu Chen's research group in 2012[13]. The concept is demonstrated using $LiMn_2O_4$ and zinc metal electrodes in an aqueous electrolyte containing two electrochemically active ions (Li^+ and Zn^{2+}). The Rechargeable Hybrid Aqueous Battery (ReHAB) operates at about 2 V and preliminarily tests show excellent cycle performance. The energy density of a prototype battery, estimated at 50-80 Wh kg^{-1}, is comparable or superior to commercial 2 V rechargeable batteries. The combined performance attributes of this new rechargeable aqueous battery indicate that it constitutes a viable alternative to commercial lead-acid system and for large scale energy storage application and it also can significantly alleviates the safety problems on lithium-ion battery as well as its advantage of low cost.

Looking into the detailed working mechanism of ReHAB, we can see on cathode side, the lithium ion is inserted into and extracted from LiMn2O4. The reaction can be expressed as follow:

$$LiMn_2O_4 \; <=> \; Li_{1-x}Mn_2O_4 + xLi^+ + xe^- \qquad (1.1)$$

During charging process, the cathode is oxidized, meaning Li ion is extracted from the $LiMn_2O_4$ tetrahedral sites. In contrast, on discharging process, the cathode is reduced, meaning Li ion is inserted into the $LiMn_2O_4$ tetrahedral sites. These two steps have been found that usually occur on Li intercalation and de-intercalation. For CV testing, in the charge curve, the first peak located at 4.05 V (Li/Li+) means an extraction of Li ions from half of the tetrahedral sites with Li-Li interaction; [14, 15] the second peak at 4.15 V (Li/Li+) means an extraction of Li ions from the other half of the tetrahedral sites without Li-Li interaction.[14, 15]

The chemical reaction mechanism is quite different at the anode side, which is mainly related to Zn electrodeposition and dissolution. Zn electrochemical reactions happened on the anode have shown below:

$$Zn <=> Zn^{2+} + 2e^- \qquad (1.2)$$

When the battery is charged, the anode is reduced, thus Zn ions are deposited to the

Zn anode side. Conversely, Zn metal dissolves into the solution in the form of Zn^{2+} ions during discharge process.

In this case, the anode and cathode appear to be undergoing their own ion transfer process during charge and discharge, when the electrolyte acts as an ion transfer medium which providing Li^{+} and Zn^{2+} sources for the electrochemical reactions. The charge and discharge process is illustrated schematically in the Figure 1.1.

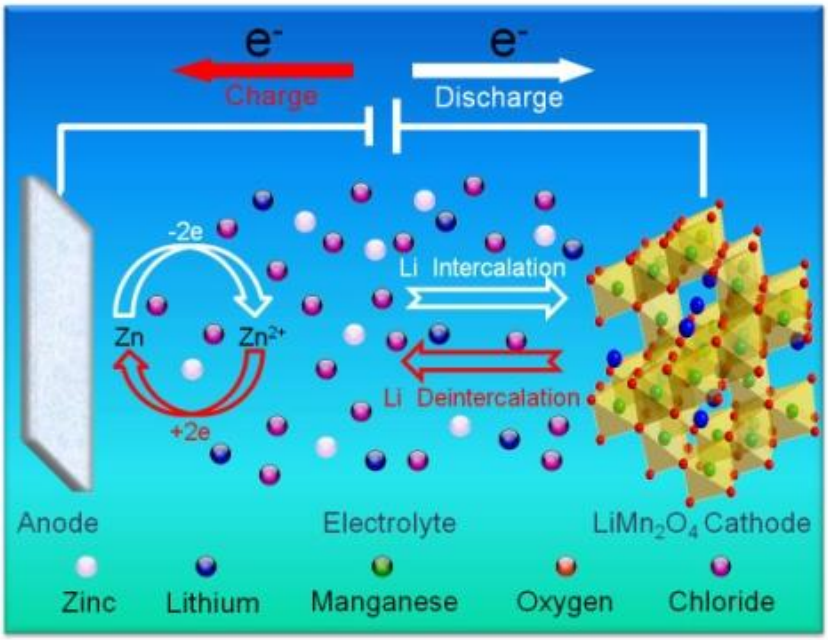

Figure 1.2: Schematic representation of the mechanism for ReHAB operation

However, all battery systems have the problem of side reactions, which constantly consume active materials (in ReHAB system, both Li^{+} and Zn^{2+} are considered to be active materials) and inevitably reduce battery life. For maintaining the capacity of the battery, the amount of electrons generated/consumed in the cathode by Li^{+} transfer should be strictly equal to the amount of electrons consumed/generated in the anode by Zn^{2+} transfer. Thus, ideally the electrons activity should only be related to the Zn deposition/dissolution and lithium-ion intercalation/de-intercalation. But in fact, in an acidic medium, both $LiMn_2O_4$ and metallic zinc may react with proton as follows [16, 17]:

$$2LiMn_2O_{4(s)} + 4H^{+}_{(aq)} \rightarrow 3MnO_{2(s)} + Mn^{2+}_{(aq)} + 2Li^{+}_{(aq)} + 2H_2O_{(aq)} \quad (1.3)$$

$$Zn + H^{+} \rightarrow Zn^{2+} + H_{2\,(g)} \quad (1.4)$$

Reaction 1.4 at the anode causes both Zn corrosion and H_2 evolution, which can seriously consume electrode active material Zn, change the electrolyte environment pH and damage the surface status of Zn anode.

On the cathode side, LiMn2O4 material has been known for not thermodynamically stable for years. At the end of discharge, Mn^{3+} is in high concentration and a disproportionation reaction may happen [18].

$$2Mn^{3+}{}_{(s)} \rightarrow Mn^{2+}{}_{(l)} + Mn^{4+}{}_{(s)} \quad (1.5)$$

Mn^{2+} generated from this reaction and dissolved into the aqueous electrolyte which can cause LMO lattice structure collapsing and thus to be an important reason for battery self-discharge [19-21].

Extra chemical reactions and self-discharge issues are the most harmful problems happened inside the ReHAB system. In the aqueous solution environment, the potential window has to be restricted within the equilibrium potential of water electrolysis reaction which is around 1.23 V [22], H_2 evolution and O_2 evolution are inevitably happened.

There are several types of reactions which could possibly generate gas, for example,

$$2H_2O \rightarrow O_{2(g)} + 4H^{+} + 4e^{-} \quad (1.6)$$

$$4OH^{-} \rightarrow O_{2(g)} + 2H_2O + 4e^{-} \quad (1.7)$$

$$2H^{+} + 2e^{-} \rightarrow H_{2(g)} \quad (1.8)$$

$$2H_2O + 2e^{-} \rightarrow H_{2(g)} + 4OH^{-} \quad (1.9)$$

It is still unclear whether one or several gas reactions happen in the ReHAB. Our research in the lab is trying to search for protective materials (especially on the anode side) to restrain the influence of the extra reactions above and using several convincing characterization methods to quantitative analysis on the performance of materials.

1.2 Electrowinning Technology

Due to the requirement of modifying the electrode materials, electro-winning technology

has been introduced to produce Zn anode. The purpose of applying electro-winning technology is to manufacture the Zn anode material having some specific electrochemical properties and surface status to meet the needs of ReHAB system that can't be realized by commercial Zn.

1.2.1 Introduction of Electrowinning

Electrowinning, also called electroextraction, is the electrodeposition of metals from their ores that have been put in solution via a process commonly referred to as leaching. Electrorefining uses a similar process to remove impurities from a metal. Both processes use electroplating on a large scale and are important techniques for the economical and straightforward purification of non-ferrous metals. The resulting metals are said to be electrowon metals.

In electrowinning, a current is passed from an inert anode through a liquid leach solution containing the metal ion so that the metal is extracted as it is deposited in an electroplating process onto the cathode. In electrorefining, the anodes consist of unrefined impure metal, and as the current passes through the acidic electrolyte the anodes are corroded into the solution so that the electroplating process deposits refined pure metal onto the cathodes. [23] Fig. 1.2 shows a typical apparatus for electrowinning copper.

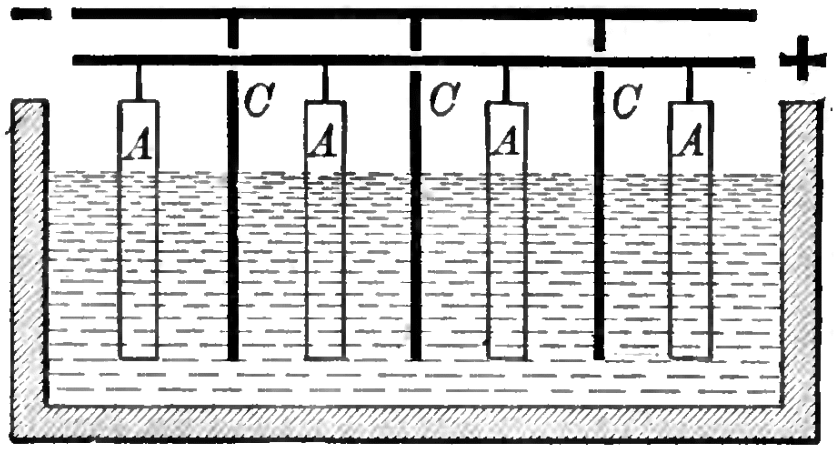

Figure 1.3: Apparatus for electrolytic refining of copper

The most common electrowon metals are lead, copper, gold, silver, zinc, aluminium, chromium, cobalt, manganese, and the rare-earth and alkali metals. For aluminum, this is the only production process employed. Several industrially important active metals (which react strongly with water) are produced commercially by electrolysis of their pyrochemical molten salts. Experiments using electrorefining to process spent nuclear fuel have been carried out. Electrorefining may be able to separate heavy metals such as plutonium, caesium, and strontium from the less-toxic bulk of uranium. Many electroextraction systems are also available to remove toxic (and sometimes valuable) metals from industrial waste streams. [23]

1.2.2 Electro winning zinc technology

Zinc is an important base metal required for various applications in metallurgical, chemical and textile industries. [24] Electro winning zinc technology is the most popular technique to produce Zn metal nowadays. In 1980s above 70% of the world's total Zn production is made by electrowinning with insoluble anodes, and this percentage has increased since then. [25]

Mineral acids, chiefly sulfuric acid, are the most common leaching reagents. Minerals are attacked more strongly when acids are hot and concentrated. The action of sulfuric acid is often sufficiently strong to make fine grinding unnecessary. Acid leaching has one special advantage if the metal is subsequently recovered by electrolysis. During electrolysis, the acid consumed in leaching is regenerated. [26]

The Zinc electrowinning technique applied on our research is based on acidic solution, which uses zinc sulfate solution as electrolyte.

① Principle of electrodeposition in zinc sulfate solution

Metal ions can be recovered from leach liquors by applying an electromotive force to the system. Positively charged metal ions will migrate toward a negatively charged pole. It should be noted that by adjusting the potential, selective deposition of meatal ions is

possible. For example, in a solution containing zinc ion and copper ion, if the electrical potential is gradually increased, the copper ion will be deposited first at a lower electrical potential because copper is a more noble metal than zinc.[27]

Industrially, zinc ores are roasted, dissolved in sulphuric acid and then highly purified. Metallic zinc is won from the purified zinc sulphate solution by electrolysis using aluminium cathodes and lead anodes. [28] Fig. 1.2 shows the apparatus setting of zinc electrowinning.

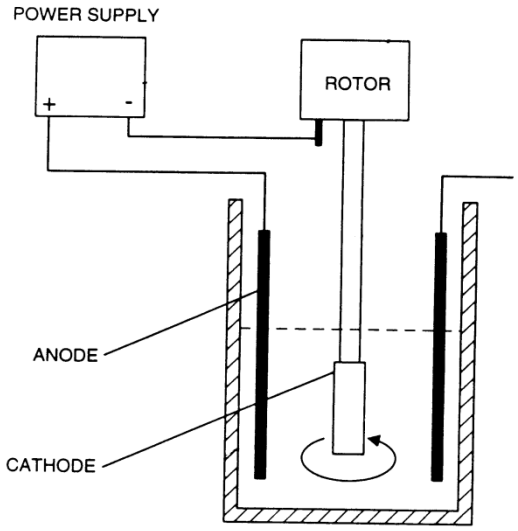

Figure 1.4: Zn Electrowinning Schematic Diagram

For easy understanding, the chemical reaction mechanism during electrowinning process has been separated into three parts: ionization reaction in electrolyser, cathode reaction and anode reaction. An assumption has been made that there are no impurities on both electrolyte and electrodes.

According to ionization theory, the ionization reaction happened on the electrolyser have shown below:

$$ZnSO_4 \rightarrow Zn^{2+} + SO_4^{2-} \quad (1.10)$$

$$H_2SO_4 \rightarrow 2H^+ + SO_4^{2-} \quad (1.11)$$

$$H_2O \rightarrow H^+ + OH^- \quad (1.12)$$

Positive ions move to the cathode and reduction reaction happened when power's on.

Zn^{2+} accepts electrons and precipitates on the cathode side:

$$Zn^{2+} + 2e^- \rightarrow Zn \quad (1.13)$$

At the same time, negative ions move to the anode and oxidation reaction happened. H_2O loses 2 electrons and O_2 evolutes on the anode side:

$$2H_2O \rightarrow 4H^+ + O_2 + 4e^- \quad (1.14)$$

Combining both reaction 1.13 and 1.14, the overal reaction is shown below:

$$2ZnSO_4 + 2H_2O \rightarrow 2Zn + 2H_2SO_4 + O_2 \quad (1.15)$$

There are also side reactions on both anode and cathode side:

$$2H^+ + 2e^- \rightarrow H_{2(g)} \quad (1.16)$$

$$Mn^{2+} + 2H_2O \rightarrow 4H^+ + MnO_{2(s)} + 2e^- \quad (1.17)$$

Generally, above 90% of the cathodic current is used in the production of zinc by reaction 1.13, and 99% of the anode current is used by reaction 1.14.[29]

It is most beneficial in connection with new or cleaned anodes, and especially with new anodes-which consist, at least in major proportion, of lead-for example the well known silver-lead anode which contains about .75 to 1% silver. [30]

The major variables that affect these reactions are: Zn^{2+} concentration, H^+ concentration, current density and temperature. [28] Additives and impurities effects also play important roles during electrowinning process. [31-41]

② Effects of current density and temperature

Generally, the higher current density promotes a random growth of electrodeposits which loosely adhere to the cathodes and are readily dislodged by the greater evolution of hydrogen gas. [42] Meanwhile, higher current density can enhance current efficiency of MnO_2 generation as showed in reaction 1.17, and therefore decreases the current efficiency of Zn deposition. [43] Low current density electrowinning carries the opposite way.

Jianming Lu *et al.*, [44] carried out zinc elelctrowinning experiments on different current density conditions. The effects of current density on current efficiency and induction time were investigated in the current density ranging from 450 to 750 Am^{-2}. The zinc deposit mass increased significantly with increasing current density from 450

to 650 Am^{-2} while it increased very little with further increasing current density to 650 A m^{-2}. Hydrogen evolution was the main cathodic side reaction. In the current density ranging from 450 to 750 Am^{-2}, the current efficiency of hydrogen evolution increased with increasing current density. At a higher cathodic current density, hydrogen evolution was facilitated more than zinc deposition, resulting in a lower zinc current efficiency.

On the other hand, conventional zinc electrowinning plants operate usually at the relatively low temperatures of 35°-40° C. and at low current densities in the range of 30-40 amp/sq. ft., building up, during electrolysis, a sulfuric acid concentration of the order of 100 g/l. This combination of operating conditions results in satisfactory current efficiencies, produces zinc plates, sufficiently low in lead content to be suitable for many important uses and yields an electrolyte bleed from the cells which has the required acidity for leaching zinc oxide concentrate, to form a fresh electrolyte feed to the cells. [45]

An optimum temperature range of 30°-40° C is maintained by cooling because ampere efficiency suffers at higher temperatures. In addition, lead contamination of the zinc cathode, originating from the conventional anode, increases with temperature. The theoretical decomposition voltage of zinc sulfate is 2.35 volts, but the commercial value with lead anodes is about 2.67 volts. Due to the existence of over potential, the actual applied voltage is in excess of 3 volts and increases with current density. [46] But maintaining the cells at 30°-40° C. usually requires expensive cooling; and operating at currents higher than about 40 ASF(amps per square foot), which is very desireable indeed to reduce the high tankhouse capital cost, is commonly ruled out because it results in excessive lead contamination of the zinc, due to anodic lead dissolution.

Researchers have also found that the process of this invention can be carried out at temperatures up to about 60℃. (Making it possible to avoid or minimize cooling) with no such lead contamination and without significant sacrifice of current efficiency. Temperatures in excess of about 75℃ are undesirable because of hydrogen reduction of sulfate to sulfide. And we have further found that the process of this invention can be carried out at current densities far in excess of the 30-40 amps/sq. ft. range, (again without causing lead contamination of the zinc) the upper limit being primarily set by economic considerations of optimizing capital and operating costs. [45]

③ Impurity effects in zinc electrowinning

The presence of impurities in the electrolyte is a major problem for the zinc electrowinning industry. Low levels of impurities greatly influence the cathodic deposition of zinc, leading to a decrease in zinc current efficiency and to changes in deposit morphology.[47] Metallic impurities more noble than zinc may affect the purity of zinc deposits by co-deposition and some of them (Co and Ni) induce the redissolution of deposited zinc.[48] However, not only the absolute magnitude of the various impurities, but also the synergistic interactions among them determine the quality of deposits from the solution.[49] Due to the incomplete explanation for the mechanism of their negative action, a promising development in this area is the application of cyclic voltammetry and of the impedance method to the investigation of the electrodeposition process.[31, 50]

L Mureşan *et al.*, [33] carried out experiments on influence of several metallic impurities on sulfate electrolyte zinc electrowinning. The results indicated that the metallic impurities affect the zinc electrodeposition process. Cd favors zinc deposition by diminishing the nucleation overpotential and it is co-deposited with zinc on an aluminum cathode. The grain size of the deposit is larger in the absence of cadmium. Fe increases the nucleation overpotential, inhibiting zinc deposition, but has no significant influence on the morphology of the deposit when glue is present. Cu has a harmful effect on zinc electrowinning. The cathodic deposit is non-adherent, consisting of porous microspheres and a parallel discharge of Cu ions takes place. Hydrogen evolution and zinc deposition are enhanced. And overall, the study suggests that, in one way or another, the metallic impurities exert a deleterious effect on zinc electrodeposition, affecting the purity of the deposit, its morphology and influencing the kinetics of the process.

The individual effects of lead, copper, nickel, cobalt and antimony on zinc electrowinning were evaluated by A. R. Ault [47] using measurements in high-purity synthetic solutions, free from additives. The coulombic efficiency (QE) of zinc electrodeposition was determined over 2 h under mass transfer-controlled conditions at a temperature of 35° C and a current density of 400 Am^{-2} in a solution of 0.8 M $ZnS0_4$ + 1.07 M H_2S0_4 . Antimony had a very detrimental effect on QE causing decreases of 5 and

50% at 4 and 14 μg l^{-1}, respectively. Antimony also exerted a strong grain-refining effect and changed the deposit orientation from random to (112) to (004) with increasing concentration. Lead had a small beneficial effect on QE at the electrode rotation rate employed (20 s^{-1}). It also exerted a grain-refining effect and changed the deposit orientation from random to (102), (103), (104), to strong basal (004), (002) with increasing concentration. Copper, nickel and cobalt had minor effects on QE, with reductions at 5 mg l^{-1} of 0.8, 0.3 and 0.3%, respectively. The effects of copper on morphology and orientation were very concentration dependent, but with a general trend towards grain-refining and random orientation. Nickel promoted coarse-grained deposits and changed the orientation from random to (114), (102) to (204), (102) with increasing concentration. Cobalt had the least effect on the morphology of the deposit, although it gradually increased the basal plane orientation with increasing concentration.

The individual effects of 15 impurities and their interaction with glue on zinc electrowinning from industrial acid sulphate electrolyte were characterized in terms of deposit morphology and preferred deposit orientation and in terms of current efficiency and zinc deposition polarization behavior by D. J. Mackinnon *et al.*. [31] The effects of 15 elements and their interaction with glue on zinc electrowinning from industrial acid sulphate electrolyte have been characterized in terms of deposit morphology and orientation and in terms of zinc deposition current efficiency and polarization behavior. It was observed that the zinc deposition CE (current efficiency) decreased with increasing atomic number of the elements in each period of the periodic table. The decrease in CE paralleled a corresponding increase in the rate of hydrogen evolution which increased with increasing atomic number in each period. The elements most detrimental to zinc deposition were Ge, Sb, Se and Te followed by Sn, As (V), Bi and Ga. As (III) had no effect on the CE of zinc deposition whereas In, Pb and Tl resulted in a slightly increase in CE. The addition of glue to the electrolyte counteracted the detrimental effects of Sb and Ge on the CE of zinc deposition. Glue had virtually no effect on the CE for zinc deposition from electrolytes containing As (III), Tl, Ga, Bi and Te. Glue, however, had a negative interaction with As (V) and Se, i.e. the CE decreased with increasing glue concentration. The glue-Sn

interaction was anomalous in that the CE decreased, reached a minimum, and then increased with increasing glue concentration.

The presence of these elements in the electrolyte also affected the zinc deposit morphology and orientation. Four distinct morphology types with corresponding orientations were observed. Additive-free electrolyte (i.e. containing no added impurities or added glue) and electrolytes containing Co, Ni, Cu, Ga, Ge, As(III), Cd and In resulted in an intermediate-type morphology consisting of well-defined zinc platelets aligned at 30-70° angles to the Al cathode. The preferred orientation was [114] [112] [102]. The presence of Tl, Pb or low concentrations of glue produced a triangular-type morphology in which the platelets were aligned at high angles -70° to the Al cathode. The preferred orientation was [101]. A vertical-type morphology, platelets aligned at -90° to the Al surface, resulted when the electrolyte contained high glue concentrations or contained both Pb and glue. The preferred orientation was [100] [110]. The basal morphology type, characterized by zinc platelets oriented at low angles (30°) to the Al cathode, resulted when the electrolyte contained Sb, Se, Te, As (V), Sn and Bi. The preferred orientation was [002] [103] [105].

The impurities also affected the zinc deposition cyclic voltammograms. Certain impurities such as Sb, Pb and Tl affected the nucleation overpotential whereas others such as As (V), Sn, Ge and Ga affected the plating overpotential. Trivalent arsenic resulted in a characteristic pre-wave prior to zinc deposition whereas Ni and Co produced a significant cathodic current in the reverse scan following zinc stripping.

④ Effects of additives in zinc electrowinning

1. Organic additives

Organic additives are used extensively in zinc electrowinning to assist in controlling the process [37]. The most common organic additive in Zn electrowinning is glue. The addition of animal glue to the zinc electrolyte used in zinc electrowinning plants seves several purposes. [51] The glue additives control cathode growth to give smooth cathode zinc deposits, inhibit the deleterious effects that impurities such as antimony have on the current efficiency of zinc electrodeposition, and decrease acid mist evolution by forming

stable foam layers on the electrolytic cell tops in conjunction with additives such as m-p-cresol. [52]

In R. C. Kerby *et al.'s* research [37], a cyclic voltammetry technique has been developed to provide a rapid, quantitative evaluation of the effectiveness of selected organic additives in minimizing the deleterious effects that impurities, such as antimony, have on zinc deposition. Results have indicated that animal glues are more effective than the other organic additives tested, which included several gums, enzymes, and amino acids, in relation to the current efficiency of zinc production. The most effective appeared to have average molecular weights in the 25,000 to 30,000 range. The effectiveness of the glues in controlling impurity effects appeared to be related to the proteose content of the glues, whereas the requirements for good levelling properties was for the glues to have a molecular weight of at least 10,000.

The effects of sodium lauryl sulphate (SLS) in the presence and absence of antimony (III) on the current efficiency, power consumption and polarization behavior of zinc have been determined by B.C. Tripathy *et al.*. [32] The results including surface morphologies and deposit crystallographic orientations were compared with glue as the addition agent. The addition of sodium lauryl sulfate to the zinc sulfate solution increased current efficiency, reduced power consumption and improved the surface morphology. Maximum current efficiency and minimum power consumption were achieved on addition of 0.02mg dm^{-3} Sb with 1mg dm-3 sodium lauryl sulfate. SLS and glue affected the cathodic polarization of zinc similarly and SLS is more effective than glue in counteracting the deleterious effects of Sb on electrowinning of zinc from acidic sulfate solution.

B.C. Tripathy *et al.* also carried on experiment on the effects of triethylbenzylammonium chloride (TEBACl) on the electrowinning of zinc from acidic sulfate solutions with the presence and absence of antimony(III).[35] The factors considered included the current efficiency (CE), power consumption, polarization behavior, and the crystallographic orientations and surface morphology of the deposits. Compared with the traditional industrial additive, glue, the addition of TEBACl increased CE, reduced power consumption and improved the surface morphology.

Maximum CE and minimum power consumption were obtained at 2mg dm^{-3} TEBACl and 0.01mg dm^{-3} Sb (III). The exchange current density, Tafel slope and transfer coefficient were determined to elucidate the nature of the electrode reactions involved.

Therefore, they continually research on the effects of the organic additives cetyltrimethylammonium bromide (CTABr) and tetrabutyl ammonium bromide (TBABr) on the electrowinning of zinc from acidic sulphate solutions with the presence and absence of trace amounts of antimony(III).[53] The results indicated that CTABr has similar properties to the commonly used industrial additive glue with respect to current efficiency, power consumption, polarization behavior, and the crystallographic orientation and surface morphology of the zinc deposits. TBABr was generally less useful with respect to all these properties. Voltammetric studies indicate that polarization for zinc electrodeposition decreased in the order CTABr>glue>TBABr. The nature of the electrode reactions were investigated through measurements of exchange current densities, Tafel slopes and transfer coefficients.

The latest research B.C. Tripathy *et al.* study on was the effects of perfluorobutyric acid, perfluoroheptanoic acid and perfluorooctanoic acid, in the presence and absence of antimony (III), on the cathodic current efficiency, power consumption and polarization behavior of the cathode during the electrowinning of zinc from acidic sulphate solutions. [34]The surface morphology and crystallographic orientations of the zinc deposits were compared between these additives. Addition of any of these perfluorocarboxylic acids increased the current efficiency, decreased power consumption and produced better surface morphologies. Voltammetric studies indicated that polarization of the electrode in the presence of these additives was in the order PFOA > PFHA > PFBA. The nature of the electrode reactions was investigated through measurements of exchange current densities, Tafel slopes and transfer coefficients. Perfluorocarboxylic acids were found to be better additives for zinc electrodeposition when Sb (III) was absent from the zinc electrolyte.

S. C. Das *et al.* [54] have investigated in the effects of 4-ethylpyridine and 2-cyanopyridine on the electrowinning of zinc in the presence and absence of antimony. The results are compared with those of a common industrial additive, gum arabic.

Addition of either compound reduced current efficiency, increased power consumption and lowered the surface quality of electrodeposited zinc. Both the additives showed similar polarization behavior to gum arabic. Addition of 0.04mg dm^{-3} antimony increased current efficiency, reduced power consumption and altered the surface morphology and crystallographic orientations. Combinations of antimony with 4-ethylpyridine produced a desirable zinc morphology with the preferred crystal orientations (1 0 1) (1 1 2) (1 0 2) (1 0 3) and resulted in very good current efficiencies, and zinc morphology and quality.

D. J. Mackinnon *et al.*, researched on the effect of thiourea, with and without glue and antimony additions, on the current efficiency (CE) and polarization behavior of zinc deposition and on the morphology and preferred orientation of the zinc deposits electrowon (at 430 A m^{-2} and 35° C) from industrial acid sulphate electrolyte (55 g l^{-1} Zn and 150 g l^{-1} H_2S0_4).[55] Increasing concentrations of thiourea in the electrolyte decreased the CE for zinc deposition; the additional presence of antimony did not significantly alter the decrease in CE but the presence of glue resulted in a further substantial decrease in CE. Thiourea changed the zinc deposit morphology and orientation, and also altered the shape of the zinc deposition cyclic voltammogram.

2. Inorganic additives

D.J. Mackinnon *et. al.*,[41] had investigated the effect of germanium on the electrowinning of zinc from industrial acid sulphate electrolyte was studied using X-ray diffraction, scanning electron microscopy and cyclic voltammetry techniques. Germanium concentrations > 0.1 mg i-1 results in severe re-solution of the zinc deposit and hence decreased the zinc deposition current efficiency. Extreme fluctuations in the current efficiency occurred as a function of electrolysis time. Cyclic voltammograms obtained for Ge-containing electrolytes were characterized by a shoulder in the reverse scan prior to the cross-over potential. Vigorous hydrogen gassing occurred at the shoulder. These results are interpreted in terms of the formation of local Zn-Ge galvanic cells. Germanium concentrations to 0.2 mg l-1 had no effect on the morphology of the 1-

h zinc deposits but the preferred orientation changed from [114] [112] for Ge-free electrolyte to [112] [110] for electrolytes containing Ge.

An investigation of the effects of some additives on zinc electrowinning from a weak acidic sulphate electrolyte has been carried out by Liana Murean *et. al*.. [56] The results indicated that the additives tested exert a beneficial effect on the quality of the zinc deposits. They increase the cathodic polarization and promote levelling. $Al_2(S0_4)_3$ influences the reduction of zinc ions, increasing the nucleation overpotential and the deposition rate of zinc on the cathode. The conjoint use of $Al_2(S0_4)_3$, animal glue and HCE results in smooth, slightly bright deposits, showed a beneficial effect of the mixture on zinc electrodeposition as Aluminium play the role of buffer and increasing the dispersion capacity of the electrolyte. The analysis of deposit purity suggested that the additives inhibit the discharge rate of impurity metal ions, such as copper and lead, whose deposition is diffusion controlled.

There are lots of other metallic additives have been investigated as show in section 1.2.2 ③.

1.3 Objective

All the studies in this thesis are examined around the ReHAB performance including battery cycle performance and float charge current. The research focused on the alternative methods of ReHAB anode by applying electrowinning technique. Zn anodes have been characterized for both morphology and electrochemical parameters. The overall objectives of this thesis can be summed as follows:

1. Produce series types of Zn plates by using eletrowinning technology. Different additives have been applied for producing Zn with different surface condition and electrochemical performance;

2. Comprehensively investigate on Zn plates by scanning electron microscope (SEM),

X-ray diffraction (XRD) and corrosion test (linear polarization method, including Tafel curve fitting);

3. Study on the influence of electrowinning Zn on battery cycle performance: Assemble battery to Swagelok™ cell, carry on battery cycle test, and do AC impedance(EIS) after cycles;

4. Study on the influence of electrowinning Zn on float charge performance: Assemble battery to Swagelok™ cell, carry on float charge test, and do elemental analysis after float charge;

5. Summarize the performance of different electrowinning Zn anodes, synthesis evaluate the feasibility of electrowinning technique to the ReHAB system.

1.4 Structure of Thesis

The thesis is organized into seven chapters.

- Chapter 1 firstly gives a basic introduction of development battery history, introduces the invention of ReHAB system and its structure & mechanism. Secondly, the chapter explains the concept of eletrowinning technique and several effects on the process.

- Chapter 2 mainly describes experimental theories and methods used in this thesis, including electrowinning theory and its apparatus, battery preparation, scanning electron microscopy technique, X-ray diffraction technique, theory and

the linear polarization method with Tafel fitting, battery cycle test, electrochemical impedance spectroscopy technique, float charge current test, and elemental analysis.

- Chapter 3 to 6 are focuses on experimental results on four different types of Zn anodes with various combinations of additives (Labeled as BG#1, TG#1, ITG#1 and hBITG#1)

- Chapter 7 summarizes conclusions on above chapters and gives recommends for further research.

Chapter 2

Experimental Methods and Instruments

2.1 Electro-winning Zn apparatus and processes

Electrowinning process is based on the overall reaction shown below:

$$2ZnSO_4 + 2H_2O \rightarrow 2Zn + 2H_2SO_4 + O_2 \quad (1.15)$$

2.1.1 Experiment preparation

Electrolyte preparation: The electrolyte was prepared using neutral zinc electrolyte, deionized water, reagent grade sulfuric acid, highly pure metallic manganese and boric acid with the composition of 60 g/L Zn($ZnSO4{\cdot}7H2O$, Alfa Aesar, ACS, 99%-103%), 160 g/L H_2SO_4(Alfa Aesar, CR), 3 g/L Mn($MnNO_3{\cdot}4H_20$, Sigma Aldrich, 98%), 20 g/L H_3BO_3(Sigma Aldrich, for electrophoresis, 99.5%) and variable amounts of additives.[47]

The various additives were introduced into the electrolyte by pipetting appropriate volumes of concentrated aqueous stock solutions[57] prepared from Bi_2O_3(Sigma Aldrich, 99.9% trace metals basis), $In_2(SO_4)_3$(Sigma Aldrich, 98%), Gelatin(Sigma Aldrich, for electrophoresis) and Thiourea(Sigma Aldrich, ACS reagent, 99%). The amounts of each additives in different experiments which have carried on in this thesis are shown in Table 2.1.

Table 2.1 Components of additives on four electrowinning Zn experiments

Labeled Name	**Components of Additives**			
	Bi_2O_3	**Thiourea**	**$In_2(SO_4)_3$**	**Gelatin**
BG#1	30 mg/L	-	-	10 mg/L
TG#1	-	30 mg/L	-	10 mg/L
ITG#1	-	30 mg/L	30 mg/L	10 mg/L
hBITG#1	15 mg/L	30 mg/L	15 mg/L	10 mg/L

The amounts of each additive are determined by both references [31-33, 37, 41, 47-56] and preliminary experiments. The range of tested additives is 5 mg/L to 100 mg/L and the best electrowinning results (combined with electrochemical tests) are always on the range of 30-50 mg/L. Considering both industrial costs and comparability, total amount of 30mg/L (not including Gelatin) organic and inorganic additives have been added in each experiment. 10 mg/L of Gelatin has significantly improved the success rate of all electrowining experiments.

The results of BG#1, TG#1, ITG#1 and hBITG#1 are represented for the effects of inorganic (Bi), organic (thiourea), 1 inorganic (In) and 1 organic (thiourea), 2 inorganic (Bi and In) and 1 organic (Thiourea), respectively.

Anode preparation: New Lead-silver alloy (0.8% silver) anodes were first sandblasted to achieve an average roughness of 30 μm, and then electrochemically conditioned for 2 weeks. The objective of sandblasting and electrochemical conditioning was to build a dense PbO_2 layer and also a dense layer of MnO_2, both of which firmly adhere to the lead

substrate. These two layers prevent the significant dissolution of lead and contamination of the zinc deposit. If the anodes were not used for a certain time, they were electrochemically reconditioned.

Cathode preparation: Aluminum plates were prepared by wet polishing sequentially on 400, 600, 1000, 2000 grit papers. Then, anodes were polished by 0.3μm Al_2O_3 powder (Boehler) dispersed in de-ionized water and a mesh (Boehler).They were sandblasted by 2000 grit paper and polished by Al_2O_3 powder again right before the electrowinning experiment. After electrowinning, aluminum anodes were stored and reused.

2.1.2 Apparatus settings

The electrolysis was run in the room temperature with stirring at a cathode current density of 60mA/cm^2. The deposition time was 240 min.

All settings were shown on Fig. 1.4.

2.2 Battery preparation

Electrolyte preparation: An aqueous electrolyte was formulated containing 2M Li_2SO_4 and 1M $ZnSO_4$, with pH adjusted to 4 by titration with 1M H_2SO_4 solution. $Li_2SO_4 \cdot H_2O$ (Alfa Aesar, 99.7%) and $ZnSO_4 \cdot 7H_2O$ (Alfa Aesar, ACS, 99%-103%) were added into deionized water under vigorous stirring. The stirring was continued overnight and the volume of obtained solution was adjusted to 500 mL for storage. Electrolyte pH was adjusted to 4.00 ± 0.05 by a few drops of 1M H_2SO_4 solution.

Anode preparation: Both Commercial zinc foil (Alfa Aesar, 99.9%) and electrowinning Zn were cleaned by deionized water and ethanol, followed by drying at 50℃ under vacuum for 5 minutes. Zinc anode was prepared from the zinc foil above by mean of electrode cutter.

Cathode preparation: Composite cathodes were prepared by casting slurries of LiMn2O4 (undoped materials from MTI Co.), acetylene black (Alfa Aesar Co., 99.9%), and polyvinylidene fluoride (PVDF, Arkema Inc.) (86:7:7 wt.%) in n-methyl-2-pyrrolidinone

(NMP, SigmaAldrich Co.) .The system was mixed by hand for 15 minutes; the mixture was cast onto a graphite foil (SGL Group Co.), and air drying at 60 ℃ for 2 h. Disks of 12 mm diameter were cut by electrode cutter (typical active material load of 2.4 mg cm^{-2}) and soaked in the electrolyte solution under reduced pressure.

Battery assembling and testing: Cathodes were immersed in electrolyte in vacuum for 20 minutes before battery assembling. AGM (Absorbed Glass Mat, NSG Co.) wet with several drops of electrolyte was used as separator. Swagelok™ type cells were used. A 12 mm in diameter stainless steel rod (SUS316) was used as an anode current collector in battery tests. The batteries were tested on a Neware battery test system (Neware Co. Ltd.).

2.3 Scanning electron microscopy (SEM)

2.3.1 Scanning electron microscopy technique

A scanning electron microscope (SEM) is a type of electron microscope that produces images of a sample by scanning it with a focused beam of electrons. The electrons interact with atoms in the sample, producing various signals that can be detected and that contain information about the sample's surface topography and composition. The electron beam is generally scanned in a raster scan pattern, and the beam's position is combined with the detected signal to produce an image. SEM can achieve resolution better than 1 nanometer. Specimens can be observed in high vacuum, in low vacuum, in dry conditions (in environmental SEM), and at a wide range of cryogenic or elevated temperatures.[58]

2.3.2 Instrument and setting

Morphological examination of the zinc deposits was determined by SEM observation. Both commercial Zn foils and electrowinning Zn plates were cut into around 3mm diameters. The microstructures of Zn were observed using scanning electron microscopy (Carl Zeiss Ultra Plus Field Emission SEM, Zeiss Co.) operating at 10 kV.

2.4 X-ray Diffraction (XRD)

2.4.1 X-ray Diffraction technique

X-ray crystallography is a tool used for identifying the atomic and molecular structure of a crystal, in which the crystalline atoms cause a beam of incident X-rays to diffract into many specific directions. Diffraction occurs when radiation is scattered by a regular array of scattering centers. By measuring the angles and intensities of these diffracted beams, a crystallographer can produce a three-dimensional picture of the density of electrons within the crystal. From this electron density, the mean positions of the atoms in the crystal can be determined, as well as their chemical bonds, their disorder and other information. [59]

Fig. 2.1 shows the conditions for diffraction x-rays by a simple crystal lattice, which are governed by Bragg's law: [60]

$$n\lambda = 2d \sin\theta \qquad (2.1)$$

d – The spacing between two adjacent planes of atoms,

n – The order of diffraction,

λ – The wavelength of the electromagnetic radiation,

θ – The scattering angle.

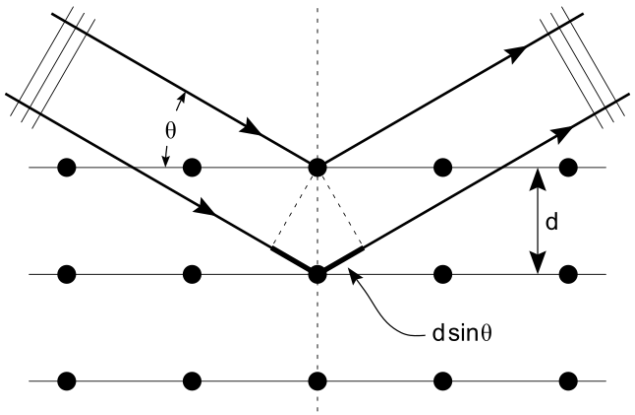

Figure 2.1 Geometry for diffraction of x-radiation

The angle θ is also called the Bragg's angle and the 2θ is referred to as the diffraction

angle (which is experimentally measured). The magnitude of the interplanar spacing is related to the Miller indices for the plane (h, k, l), which are the reciprocal of the cartesian coordinates of the plane. The schematic of the experiment in XRD is shown in Fig. 2.2. The diffraction patterns of the samples are recorded through the scanning radiation detector to the computer. Therefore, profiles of the sample can be analyzed by the computer software comparing it to a large collection of known diffraction patterns.

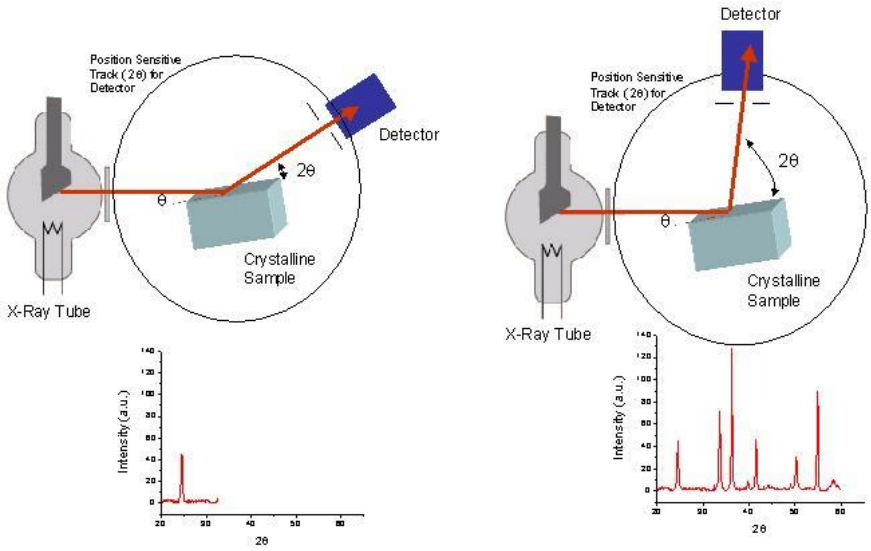

Figure 2.2 Schematic of the XRD experiment

2.4.2 Operations and settings

Electrowinning Zn and commercial Zn x-ray diffraction (XRD) patterns were collected using D8 Discover (Bruker Co., CuKa 1.5406 Å, 40 kV, and 40 A) equipped with LynxEye detector, at scan rates of 2^{o} min^{-1} after washing by dio-water and ethanol.[61, 62] Preferential orientation of the crystals was determined using a method based on X-ray diffraction. [63]

2.5 Zn corrosion

2.5.1 Principle of Zn corrosion polarization curve

When a metal specimen is immersed in a corrosive medium, both reduction and oxidation processes occur on its surface. Typically, the specimen oxidizes (corrodes) and the medium (solvent) is reduced. In acidic media, hydrogen ions are reduced. The specimen must function as both anode and cathode and both anodic and cathodic currents occur on the specimen surface. Any corrosion processes that occur are usually a result of anodic currents.

When a specimen is in contact with a corrosive liquid and the specimen is not connected to any instrumentation – as it would be "in service" – the specimen assumes a potential (relative to a reference electrode) termed the corrosion potential, E_{CORR}. A specimen at E_{CORR} has both anodic and cathodic currents present on its surface. However, these currents are exactly equal in magnitude so there is no net current to be measured. The specimen is at equilibrium with the environment. E_{CORR} can be defined as the potential at which the rate of oxidation is exactly equal to the rate of reduction.

It is important to stress that when a specimen is at E_{CORR} both polarities of current are present. If the specimen is polarized slightly more positive than E_{CORR}, then the anodic current predominates at the expense of the cathodic current. As the specimen potential is driven further positive, the cathodic current component becomes negligible with respect to the anodic component. A mathematical relationship exists which relates anodic and cathodic currents to the magnitude of the polarization [64, 65]. Obviously, if the specimen is polarized in the negative direction, the cathodic current predominates and the anodic component becomes negligible.

Tafel extrapolation and polarization resistance are two methods to quantify corrosion rates from experimental linear polarization data. For an electrochemical reaction under activation control, polarization curves exhibit linear behavior in the E Vs log (i) plots, also called Tafel behavior. Polarization behavior of Zn in acid solution is illustrated below.

$$Zn \rightarrow Zn^{2+} + 2e^{-} \qquad (2.2)$$

$$H^+ + 2e^- \rightarrow H_{2(g)} \quad (2.3)$$

Typical cathodic polarization curves with respect to Tafel behaviour are also given. Extrapolation of cathodic and anodic Tafel slopes back to the corrosion potential (E_{corr}) are shown. Intersection point corresponds to corrosion current density (i_{corr}) or corrosion rate (Fig. 2.3).

$$i_a = i_c = i_{corr} \text{ (mixed potential theory)} \quad (2.4)$$

Steady state polarization curves need be obtained to be more representative of corrosion reactions. Potentiostatic and galvanostatic methods need be compared to ascertain the choice of a better technique to determine corrosion rates. There are some demerits in Tafel extrapolation. Since polarization curves are not reversible and are influenced by experimental and environmental conditions, Tafel constants can vary from system to system. Often anodic curves may not exhibit linear behavior near Ecorr. To determine values of E_{corr} and i_{corr}, extrapolated linear sections from the anodic and cathodic curves are used. E_{corr} and i_{corr} values can be directly determined from the cross-over point (Fig. 2.3).

Tafel constants (βa and β_c) are calculated from the anodic and cathodic slopes.

At the corrosion potential (E_{corr}), the rate of hydrogen reduction is equal to rate of metal dissolution. Corrosion rate (i_{corr}) in terms of current density can be estimated. Tafel constants (β_a and β_c) can be calculated from anodic and cathodic portions of the Tafel plots.

During the activation polarization, general metal corrosion rate equation is:

$$I = i_a - i_c = i_{corr}[\exp(\frac{\varphi - \varphi_c}{\beta_a}) - \exp(\frac{\varphi_c - \varphi}{\beta_c})] \quad (2.5)$$

I – Total current

i_a – anodic current,

i_c – cathodic current,

β_a – anodic Tafel constants,

β_c – cathodic Tafel constants.

So that,

$$I = i_{corr}[\exp(\frac{\Delta E}{\beta_a}) - \exp(\frac{-\Delta E}{\beta_c})]$$

(2.6)

Tafel linear extrapolation: on strong anode polarized area, i_k=0

$$I = i_a = i_{corr} \exp(\frac{\Delta E}{\beta_a}) \tag{2.7}$$

Rewrite the equation to logarithmic：

$$\Delta E = \beta_a \ln \frac{I}{i_{corr}} = b_a \lg \frac{I}{i_{corr}} \tag{2.8}$$

On strong anode polarized area, ΔE <0, i_k=0,

$$I = -i_{corr} \exp(\frac{-\Delta E}{\beta_c}) \tag{2.9}$$

Rewrite the equation to logarithmic:

$$-\Delta E = \beta_c \ln \frac{|I|}{i_{corr}} = b_c \lg \frac{|I|}{i_{corr}} \tag{2.10}$$

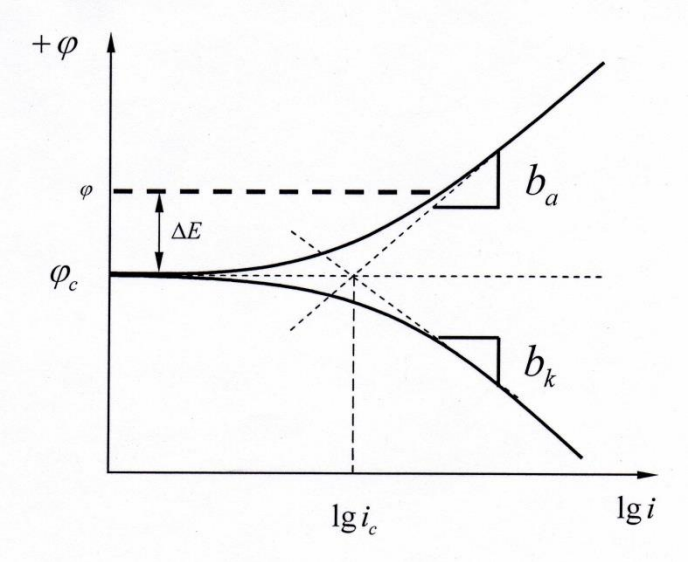

Figure 2.3 Basic principle of Tafel extrapolation on metal corrosion current test

2.5.2 Experiment setup

A three electrode testing system has been introduced to Zn corrosion evalution. The design of the three electrode electrochemical cell shows on Fig. 2.4 (a) & (b)

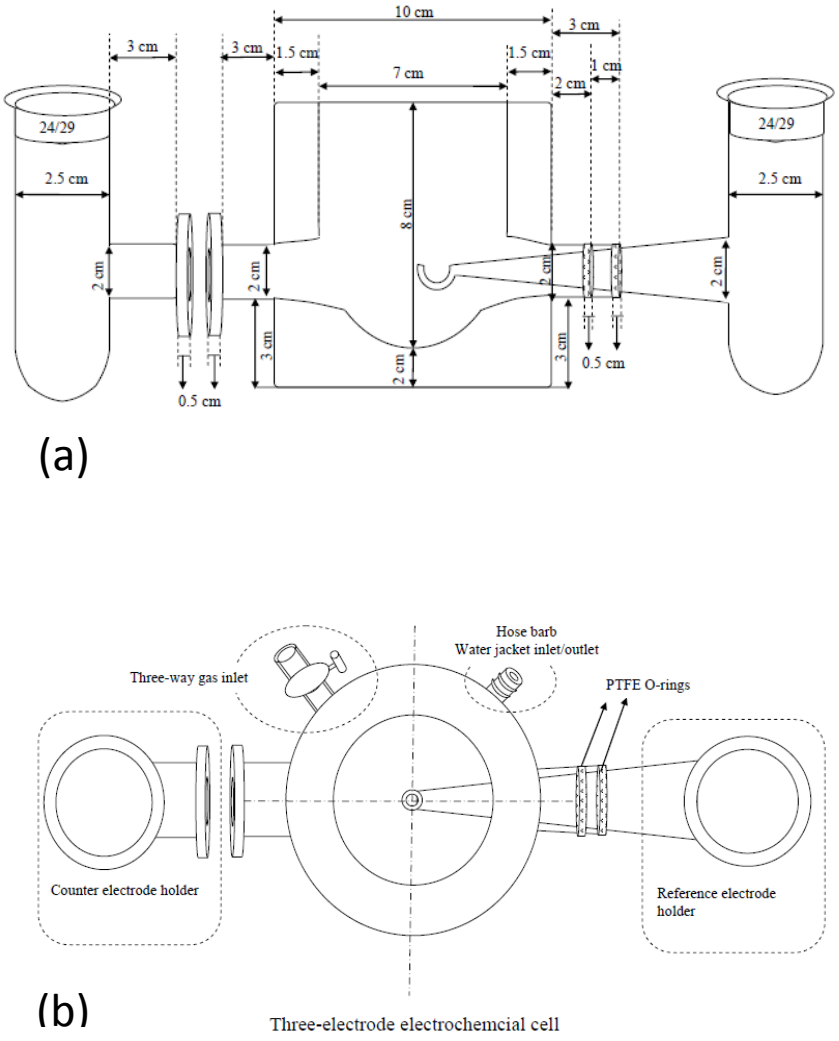

Figure 2.4 Design of three electrode eletrochemical cell: (a) Lateral view; (b) Top view.

Three electrode polarization curves were recorded under potentiostatic conditions. The tests were performed with a VMP3 controller (Bio-Logic Science Instruments Co.) during potential scanning from -1.0 to -1.5 V/SCE with a rate of 0.2 V ·min^{-1}. The Tafel curves were recorded as log I against E plots using a X-Y recorder.

A Pt counter-electrode and a Hg_2SO_4/Hg reference electrode were used. The working electrode was a rotating-disk electrode (RDE) made of Zinc (Zn anode, 0.68 cm^2, both commercial Zn and electrowinning Zn), which was prepared by electrowinning process as described on section 2.1. The rotation speed was 170 min^{-1}. Zinc anodes have been washed by both deionized water and ethanol, then dried on the oven at 50 ℃ for 5 min right before the corrosion test. The electrolyte used in these experiments had the same

composition as the electrolyte used during the battery preparation step on section 2.2.

2.6 Battery cycle test

2.6.1 Necessity of battery cycle test

Battery performance deteriorates over time whether the battery is used or not. This is known as "calendar fade". Performance also deteriorates with usage and this is known as "cycle fade"

Battery cycle life is defined as the number of complete charge - discharge cycles a battery can perform before its nominal capacity falls below 80% of its initial rated capacity. Key factors affecting cycle life are time *t* and the number *N* of charge-discharge cycles completed. Battery cycle test is an important evaluation which always determines whether the battery is durable or can be commercialized.

2.6.2 Experiment setup

Two-electrode Swagelok™ type cells [66] assembled using stainless-steel (SUS316) anode current collector and composite cathode disks (2.5 mg/cm^{-2}) separated by AGM (Absorbed Glass Mat, NSG Co.) as shown on section 2.2.

The batteries were tested on a Neware battery tester [67] (Neware Battery Test System, Neware Co. Ltd., China). Galvanostatical charge and discharge were controlled between 1.4 V and 2.1 V. Each cycle consists of a rest period of 1 minute, constant current charge at 4C rate (1 C =118 mA g^{-1}), and rest for 1 minute, followed by constant current discharge at 4C rate at 25℃. After 300 cycles testing, batteries were evaluated by discharge capacity retention. Then batteries were examined on EIS as shown in section 2.7.

2.7 Electrochemical Impedance Spectroscopy (EIS)

The purpose of the test is investigating on the influence of different Zn anode (both commercial Zn and electrowinning Zn) to the battery resistance change after certain cycles of running.

2.7.1 Introduction to Electrochemical Impedance Spectroscopy

Electrochemical Impedance Spectroscopy (EIS), also known as AC impedance methods, are widely used to characterize the electrode processes and complex interfaces. EIS is an experimental technique which measures the small sinusoidal (AC) current (or voltage) signal of known amplitude and frequency (the perturbation) to an electrochemical cell at a steady bias potential (or current). EIS is also used to monitor AC amplitude and phase response of the cell. From the measurement information about the interface, its structure and reactions taking place can be inferred. Equivalent circuit analysis of the EIS response provides information on electrode properties like bulk resistance, charge transfer resistance, diffusion and double layer capacitance, etc. [68] The following equation shows the relationship between AC voltage and frequency:

$$E_t = E_0 \sin(\omega t) \tag{2.11}$$

E_t – The potential at the time t,

E_0 – The amplitude of the signal,

ω – The angular frequency.

Angular frequency ω (expressed in radians/second) can be associated with the frequency f (expressed in hertz):

$$\omega = 2\pi f \tag{2.12}$$

In a linear system, the response signal can be described as:

$$I_t = I_0 \sin(\omega t + \varphi) \tag{2.13}$$

Combining equations 2.11, 2.12 and 2.13 into Ohm's Law, the impedance of the system can be calculated as:

$$Z = \frac{E_t}{I_t} = \frac{E_0 \sin(\omega t)}{I_0 \sin(\omega t + \varphi)} = Z_0 \frac{\sin(\omega t)}{\sin(\omega t + \varphi)} \tag{2.14}$$

Using Euler's relationship:

$$\exp ja = \cos a + j \sin a \quad (2.15)$$

The impedance can be treated as a complex function:

$$Z\omega = \frac{E}{I} = Z_0 e^{-j\varphi} = Z_0(\cos\varphi - j \sin\varphi) \quad (2.16)$$

Hence, the EIS measurements can be represented graphically through relations between the imaginary and real parts of the impedance (Fig. 2.5). This plot is known as the "Nyquist or Argand plot", where the low frequency data is shown on the right and high frequency data is shown on the left. The angle between the vector Z and the x-axis is known as the phase angle. [69]

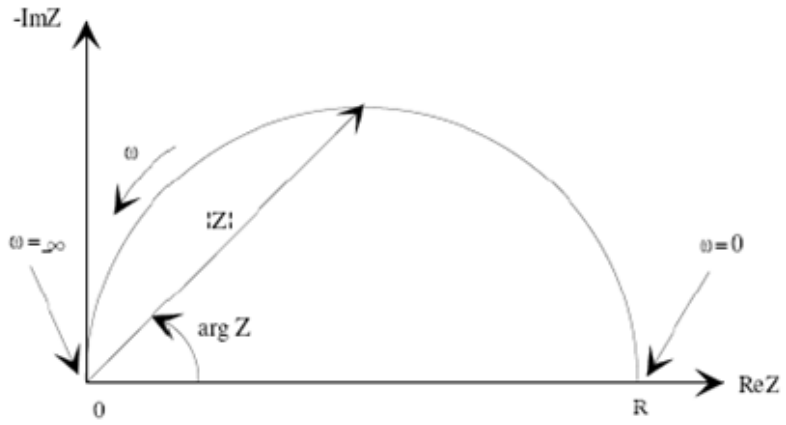

Figure 2.5 Nyquist plot with impedance vector

2.7.2 Experiment setup

Electrochemical impedance spectroscopy tests of batteries were carried on after 300 cycles running as described on section 2.6.

All EIS measurements were performed with a VMP3 controller (Bio-Logic Science Instruments Co.) at the frequency range from 0.1 Hz to 1.0 MHz using the SwagelokTM type cells, as mentioned on section 2.2.

2.8 Float charge current

The purpose of the test was investigating on the influence of different Zn anode (both commercial Zn and electrowinning Zn) to the float charge current on room temperature and high temperature.

2.8.1 Introduction to float charge

Float voltage is the voltage at which a battery is maintained after being fully charged to maintain that capacity by compensating for self-discharge of the battery. The voltage could be held constant for the entire duration of the cell's operation (such as in an automotive battery) or could be held for a particular phase of charging by the charger.[70] The appropriate float voltage varies significantly with the chemistry and construction of the battery, and ambient temperature. [71]

The float charge compensates for the loss caused by self-discharge. Float charge current value represents for how severe the side reaction is. Researchers have always tried to minimize the value of float charge current. [72-76] With the appropriate voltage for the battery type and with proper temperature compensation, a float charger may be kept connected indefinitely without damaging the battery.

2.8.2 Experiment setup

A float charge current test was performed by charging the cell to 2.1V and holding it at that voltage for a period of time on Neware battery tester (Neware Battery Test System , Neware Co. Ltd. , China), after which the float charge current was recorded. Batteries were prepared as described on section 2.2. Both commercial Zn and electrowinning Zn anode batteries have been tested.

The protocol for float charge at room temperature is: 0.2 C rate for 3 cycles and float charge for one week (168 hours) at 25 ℃. While the protocol for float charge at high temperature is 0.2 C rate for 3 cycles and float charge for one day (24 hours) at 60 ℃.

2.9 Elemental Analysis

High temperature or high voltage of float charge can damage the micro structure of cathode material (LMO). One symptom of the damage is the loss weight of conductive material which is carbon. So that by monitoring the carbon loss of on the cathode after float charge, we could compare the destruction situation of different battery to some extent.

The percentage change of carbon was estimated by elemental analysis (Vario MICRO CUBE, Elementar Co., German) after float charge experiment mentioned above on section 2.8. Cathode material has been washed by both deionized water and ethanol, then dried on the oven at 50 ℃ for 15 min.

Chapter 3

Performance of Electro-winning Zinc BG#1 on ReHAB

The Effect of Bi on electrochemical properties of Zn is investigated in this chapter. 30mg/L Bi_2O_3 and 10mg/L gelatin have been added into the eletrowinning electrolyte during process 2.1. The range of 5 mg/L to 100 mg/L Bi has been tested. The best electrochemical results were obtained at the range of 30 mg/L to 50 mg/L. Considering both industrial costs and comparability, total amount of 30mg/L Bi have been added in the experiment. All results are been compared with commercial Zn.

3.1 XRD & SEM test on Electro-winning Zn BG#1

3.1.1 XRD Results

The XRD patterns of both commercial Zn and BG#1 have been presented and compared on Fig.3.1.

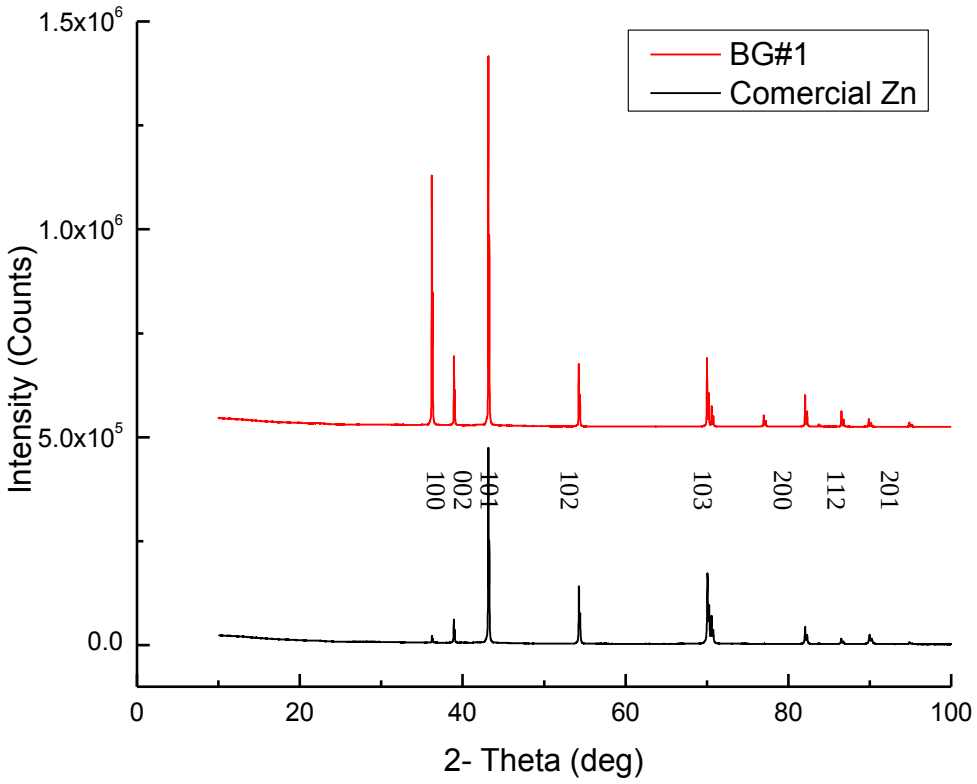

Figure 3.1 Comparison of XRD pattern:

Red plot on the top: BG#1 anode; Black plot on the bottom: Commercial Zn anode.

From the above XRD pattern, it could be observed that both samples are pure Zn. However, different from commercial Zn, the intensities of planes (100) (002) and (101) on BG#1 are much higher, while other crystal orientation changes are observed that in which the planes (102), (200), (112), (201) all show intensities similar to commercial materials. It has been widely accepted that Zn are usually characterized by the formation of fine-grained, non-porous, ductile deposits when the crystal orientation is either

random or the (101) orientation predominates. By contrast, unsatisfactory conditions are usually associated with porous, brittle and coarse-grained deposits, in such cases the (110), (100), (211), and (112) crystal orientations predominate[47, 77].

The results indicate the electrowinning Zn with Bi and gelatin as additives prefer to grow along certain direction. The different intensities of peaks also indicate different crystal orientation.

3.1.2 SEM Test Results

SEM images with different magnification are shown in Fig. 3.2. On relative lower magnification, commercial Zn shows cutting marks which might be caused by cutting process with the manufacturer. BG#1 shows relative uniform surface on X1000 magnification. On relatively higher magnification, the morphology of BG#1 could be described as a typical basal type[31] and characterized by the formation of flat hexagonal & non-porous deposits, while commercial Zn do not show any deposition type. The morphology of BG#1 is corresponded to its planes (100) and (101) both have high intensities.

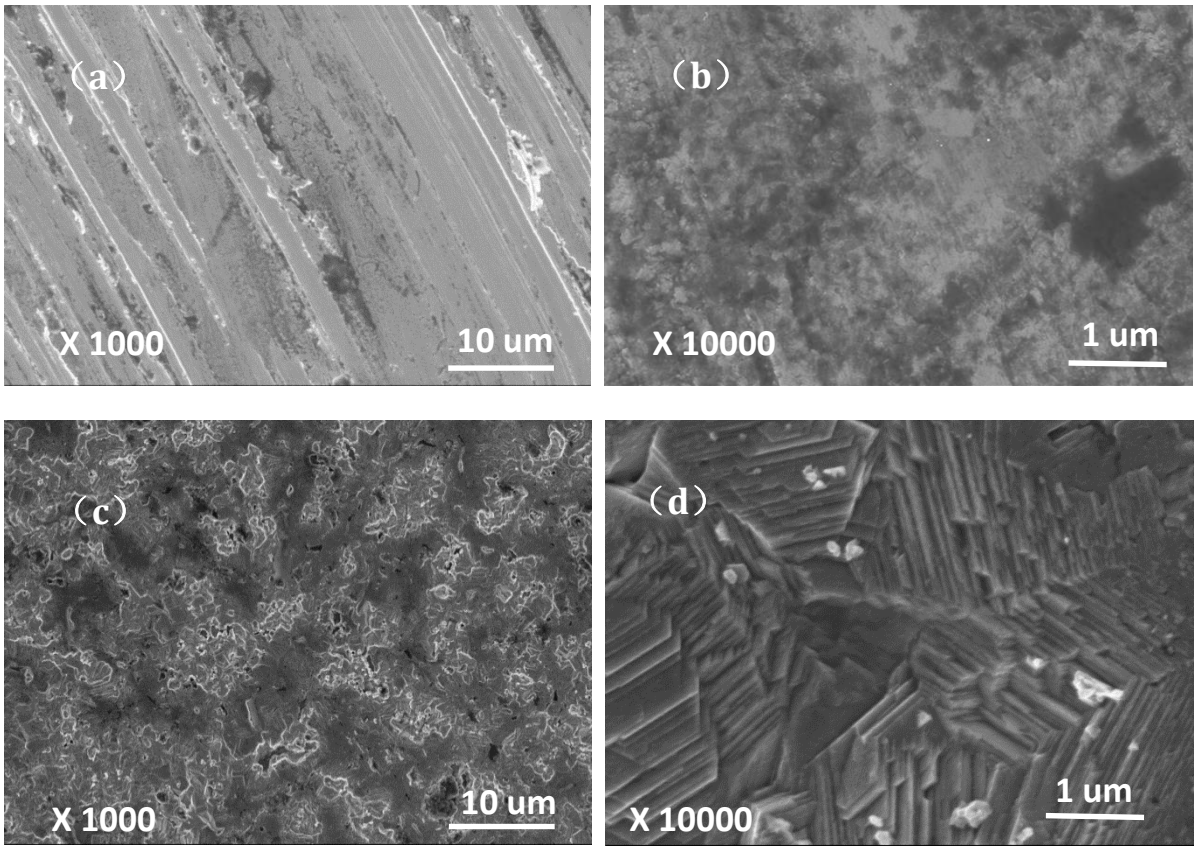

Figure 3.2 SEM image of Zn anode:

(a) Commercial Zn at X1000 magnification; (b) Commercial Zn at X10000 magnification;

(c) BG#1 at X1000 magnification; (d) BG#1 at X10000 magnification

3.2 Corrosion Test by Using Linear Polarzation

Fig. 3.3 shows the Tafel plot result of commercial Zn and BG#1 respectively, while Table 3.1 give the accurate parameter value. The corrosion current I_{corr} can be calculated from the measured polarization curve based on equations on Section 2.5.

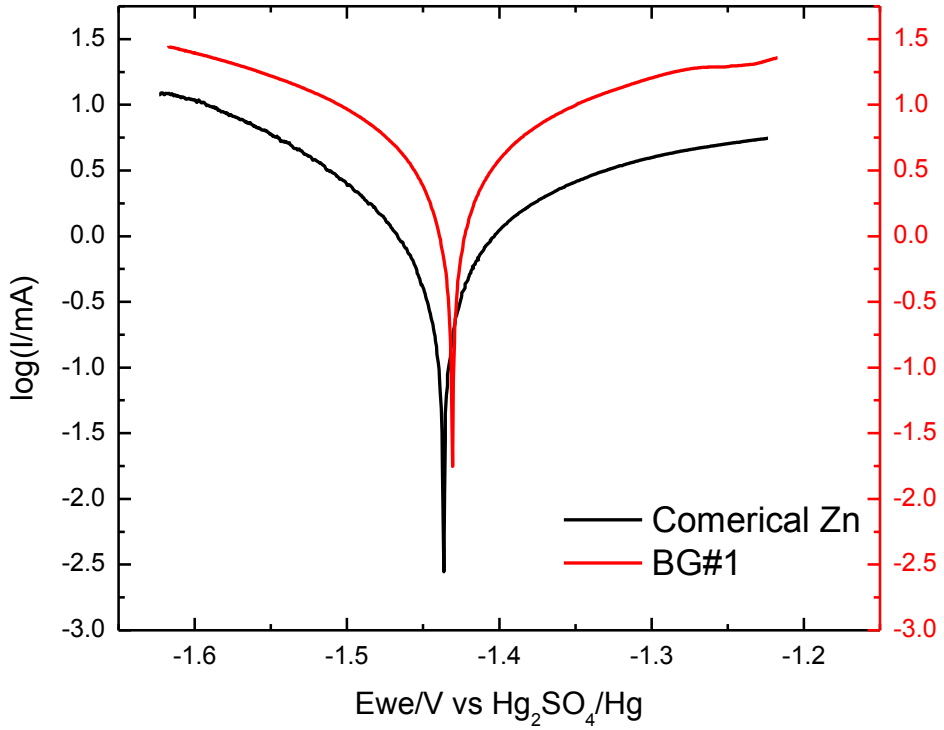

Figure 3.3 Tafel plot result of Zn anodes:

Black line on the bottom: Commercial Zn; Red line on the top: BG#1

From Table 3.1, the anode BG#1 exhibits similar corrosion potential and almost 3.6 times higher corrosion current compare to commercial Zn. The polarization resistance R_p can be calculated by the equation following below: [78]

$$R_p = \frac{B}{I_{corr}} \qquad (3.1)$$

Where B is a factor which determined by anode polarization Tafel slope β_a and cathode polarization Tafel slope β_c:

$$B = \frac{\beta_a \beta_c}{2.3(\beta_a + \beta_c)} \qquad (3.2)$$

Substituting the values on Table 3.1, the polarization resistance of commercial Zn is 35.85 Ω, while the polarization resistance of BG#1 is 10.63 Ω. It means that the anode BG#1 had the relative worse corrosion resistance compare to commercial Zn.

Table 3.1 Comparison of Tafel fit results on commercial Zn and BG#1

	E_{corr}	I_{corr}	β_c	β_a
Commercial Zn	-1 436.570 mV	1 360.753 uA	180.2 mV	296.8 mV
BG#1	-1 430.073 mV	4 863.440 uA	227.0 mV	249.9 mV

3.3 Battery Cycle performance and Electrochemical Impedance Spectroscopy (EIS)

3.3.1 Battery cycle performance

Battery cycle test has been carried on batteries using commercial Zn and BG#1 as the anodes for 300 cycles. After 200 and 300 cycles, battery capacity retention is recorded in order to qualitative evaluate battery performance, respectively. Four parallel cells are tested under the same conditions to grasp their performance dispersion.

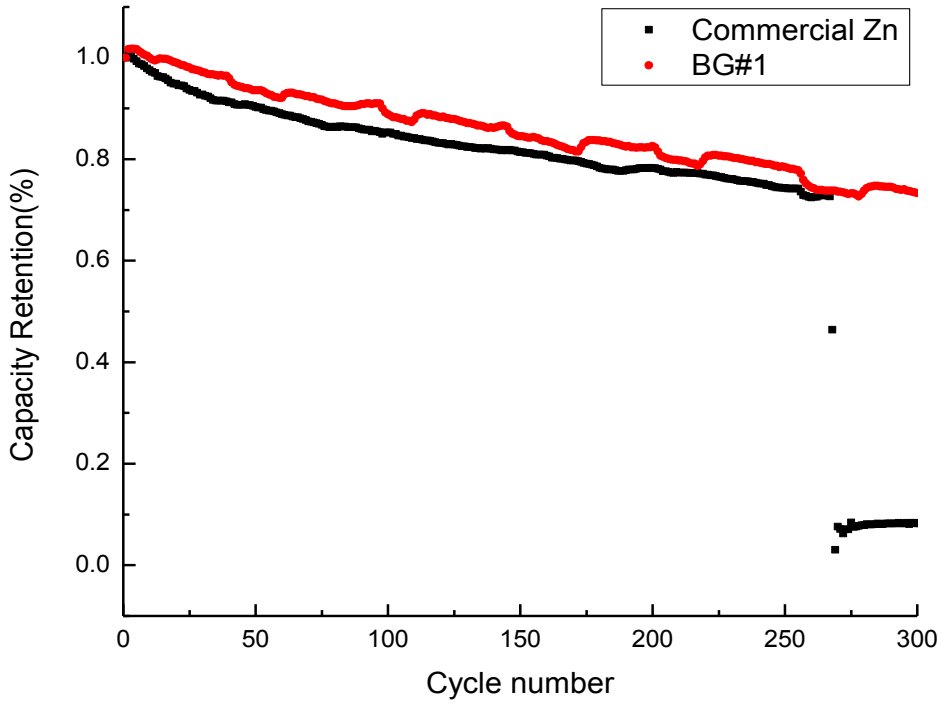

Figure 3.4 Galvanostatic charge/discharge cycle performance of ReHAB system with commercial Zn and BG#1 anodes.

As shown in Fig. 3.4, after 200 cycles running, batteries using commercial Zn anodes had capacity retention of 78.2%, yet batteries with BG#1 anodes had 82.6% capacity retention. While after 300 cycles running, batteries with BG#1 anodes had 73.2% capacity retention, yet batteries using commercial Zn anodes were all dead between 220-270 cycles. It means BG#1 was a relative better anode material on battery cycle.

3.3.2 Electrochemical Impedance Spectroscopy (EIS)

Electrochemical impedance profiles have been collected on both commercial Zn and BG#1 after cycles test in the above section.

Fig. 3.5 displays the Nyquist plots of the EIS measurement for batteries using commercial Zn and BG#1 as anode after cycles.

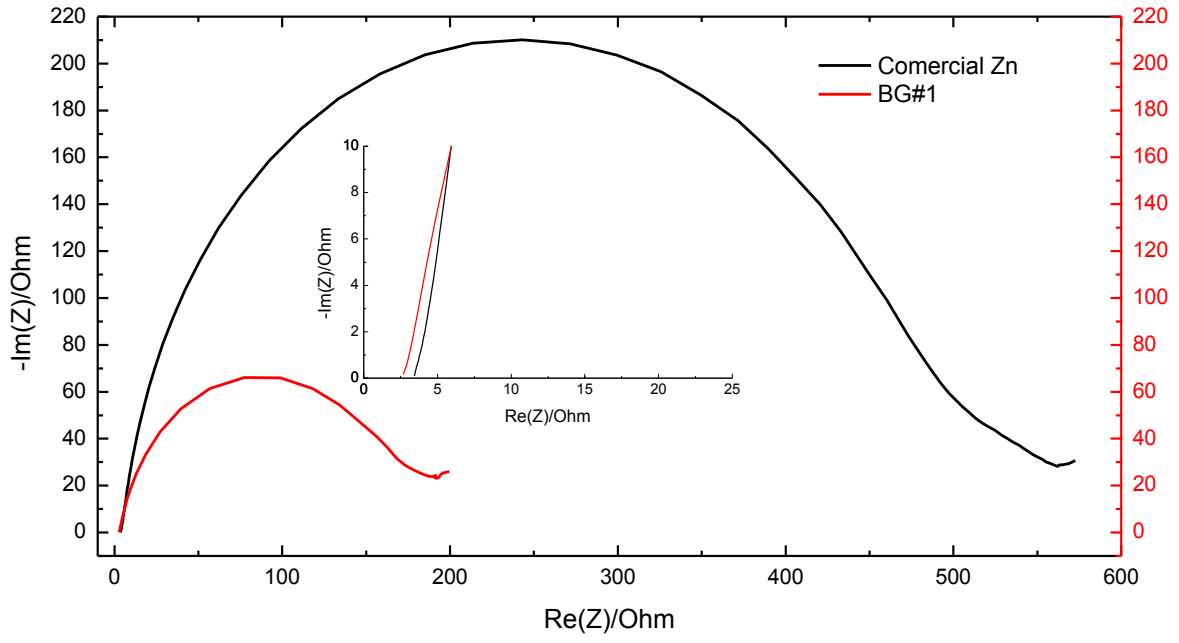

Figure 3.5 EIS profile of ReHAB anodes after 300 cycle test:

Black line on the top: Commercial Zn; Red line on the bottom: BG#1

Comparing two plots, it could be seen that the polarization resistances measured by EIS

for commercial Zn and BG#1 perform the same trend. Furthermore, battery using commercial Zn anode has much higher polarization resistance than one using BG#1 which means the former ones consumes more energy during charge-discharge process.

3.4 Float Charge Current and Elemental Analysis

3.4.1 Float Charge Current

Float charge current test has been carried on between commercial Zn and BG#1 at both room temperature (25 ℃) and high temperature (60 ℃). After float charge, float current is recorded in order to qualitative evaluate on battery performance. Four parallel cells are tested under the same conditions to grasp their performance dispersion.

Fig. 3.6 showed the result of float charge currents of batteries using commercial Zn and BG#1 at two temperatures.

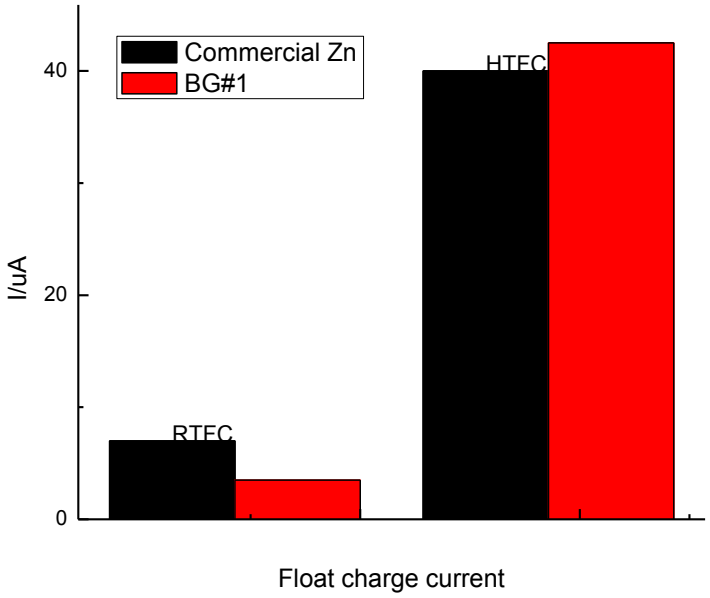

Figure 3.6 Float charge current on room temperature(RTFC) and high temperature(HTFC) for commercial Zn and BG#1

At room temperature (25 ℃), float charge current of commercial Zn is almost twice of BG#1 which means less side reactions happened on batteries using BG#1 anode. While at high temperature (60 ℃), float charge current of commercial Zn was slightly less than of BG#1 which means less side reactions happened on batteries with commercial Zn anode. Batteries with BG#1 anodes exhibit better room temperature float charge performance, while batteries with commercial Zn anodes show slightly better high temperature float charge performance.

3.4.2 Elemental analysis

Elemental analysis have been conducted on cathodes for both commercial Zn and BG#1 anode batteries after float charge test in the above section. Carbon percentages in cathodes are recorded in order to qualitative evaluate on side reaction during float charge experiment.

Fig. 3.7 shows carbon percentage of cathode material after both room temperature and high temperature float charge.

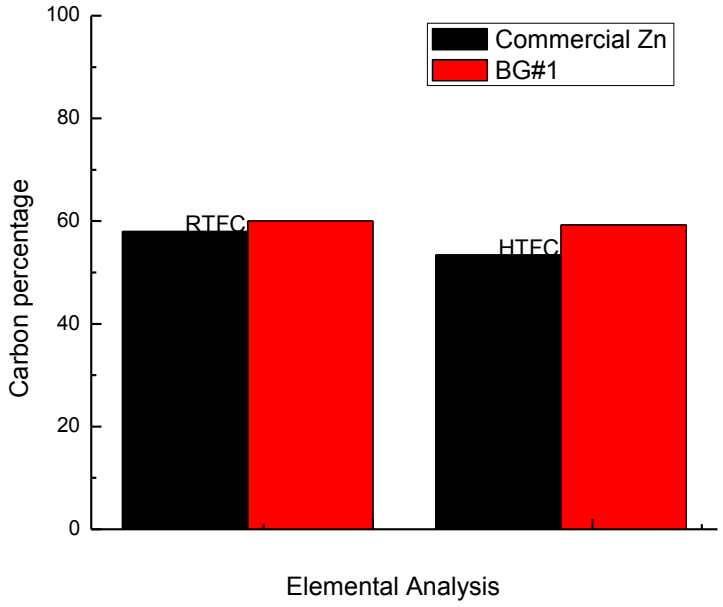

Figure 3.7 Carbon percentage of cathode material after float charge at room temperature (RTFC) and high temperature (HTFC) for commercial Zn and BG#1

Results indicate that batteries with BG#1 anode had more carbon on cathode material after both RTFC and HTFC which suggest that batteries using BG#1 anode stabilizes the cathode material better during float charge process. The underlying reason is because less carbon consumption means less oxygen evolution (to react with carbon or destroy the original structure) and thus, the integrity of cathodes is sustained and the batteries are more stable when functioning.

3.5 Summary for BG#1 anode

3.5.1 Characterization of electrowinning Zn and Commercial Zn

The XRD pattern results indicate that the electrowinning Zn with Bi and gelatin as additives prefer to grow along certain direction. The different intensity of peaks also indicated different crystal orientation. The intensities of planes (100) (002) and (101) on BG#1 are much higher, while the planes (102), (200), (112), (201) all show intensities similar to commercial materials. SEM images on relative lower magnification, commercial Zn showed cutting marks which might be caused by the cutting process with manufacturer. BG#1 showed relative uniform surface on X1000 magnification. On relative higher magnification, the morphology of BG#1 could be described as a typical basal type and characterized by the formation of flat hexagonal & non-porous deposits, while commercial Zn do not show any deposition type.

Since Zn are usually characterized by the formation of fine-grained, non-porous, ductile deposits when the crystal orientation is either random or the (101) orientation predominates and unsatisfactory conditions are usually associated with porous, brittle and coarse-grained deposits, in such cases the (110), (100), (211), and (112) crystal orientations predominate, the morphology of BG#1 is corresponded to its planes (100) and (101) both have high intensities.

3.5.2 Electrochemical performance

The anode BG#1 is characterized by similar corrosion potential and almost 3.6 times higher corrosion current compare to characteristics of commercial Zn. It means that the anode BG#1 has the relatively worse corrosion resistance.

After 200 cycles, batteries using commercial Zn anodes had capacity retention of 78.2%, yet batteries with BG#1 anodes had 82.6% capacity retention. While after 300 cycles running, batteries with BG#1 anodes had 73.2% capacity retention, yet batteries using commercial Zn anodes were all dead between 220-270 cycles. It means BG#1 was a relative better anode material on battery cycle.

The polarization resistances measured by EIS for commercial Zn and BG#1 has the same trend. It also could be seen that the battery with commercial Zn anode has much higher polarization resistance than BG#1 which means the former ones consumes more energy during charge-discharge process.

At room temperature (25 ℃), float charge current of commercial Zn is almost twice of BG#1 which means less side reactions happening on batteries using BG#1 anode. While at high temperature (60 ℃), float charge current of commercial Zn was slightly less than of BG#1 which means less side reactions happened on batteries using commercial Zn anode at this temperature. Results of elemental analysis indicate that batteries with BG#1 anode has more carbon on cathode material after both RTFC and HTFC which suggest those with BG#1 anode are more stable on cathode material during float charge process.

Based on the results above, the advantages on battery performance of BG#1 anodes could be attributed to the uniform deposits, preferable crystal orientations and high corrosion resistance. The relative flat surface could inhibit Zn dendrite formation during battery cycle test and could also provide uniform current distribution which is important on float charge process.

Chapter 4

Performance of Electro-winning Zinc TG#1 on ReHAB

The Effect of thiourea on electrochemical properties of Zn is investigated in this chapter. 30mg/L thiourea and 10mg/L gelatin has been added into the eletrowinning electrolyte during process 2.1. The range of 5 mg/L to 100 mg/L thiourea has been tested. The best electrochemical results were obtained at the range of 20 mg/L to 30 mg/L. Considering both industrial costs and comparability, total amount of 30mg/L thiourea have been added in the experiment. All results are compared with those of commercial Zn.

4.1 XRD & SEM test on Electro-winning Zn TG#1

4.1.1 XRD Results

The XRD patterns of both commercial Zn and TG#1 have been compared on Fig.4.1.

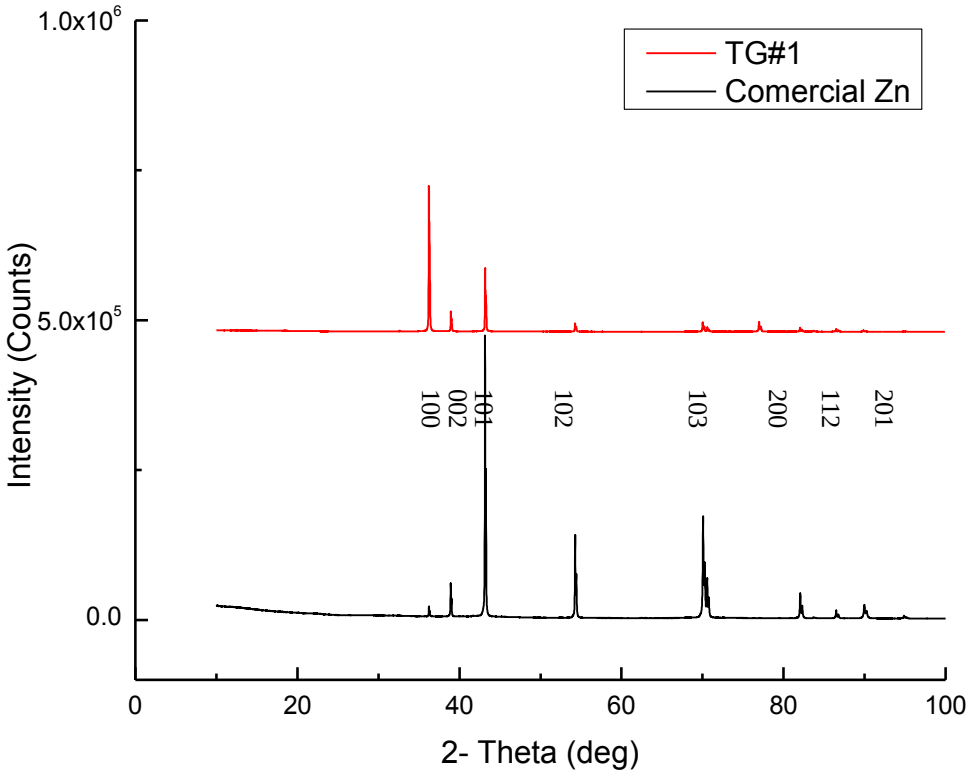

Figure 4.1 Comparison of XRD pattern :

Red plot on the top: TG#1 anode; Black plot on the bottom: Commercial Zn anode.

From the above XRD pattern, it could be observed that both samples are pure Zn. However, different with commercial Zn, the intensities of planes (100) and (002) on TG#1 are much higher, while other crystal orientation changes are observed that in which the planes (101), (102), (200), (112), (201) all showed lower intensities.

The results indicate the electrowinning Zn with thiourea and gelatin as additives prefers to grow along certain directions. The different intensity of peaks also indicated different crystal orientation.

4.1.2 SEM Test Results

SEM images with different magnification are shown in Fig. 4.2. Comparing to commercial Zn on Fig. 3.2(a)&(b), on relatively lower magnification, TG#1 anode shows relative uniform surface on X1000 magnification. On relatively higher magnification, the morphology of TG#1 could be expressed as a mixed basal type[31] and characterized by the formation of fine-grained & porous deposits. The porous deposits might relate to the high intensity of plane (100) and fine-grained morphology is determined by lower intensities of various planes.

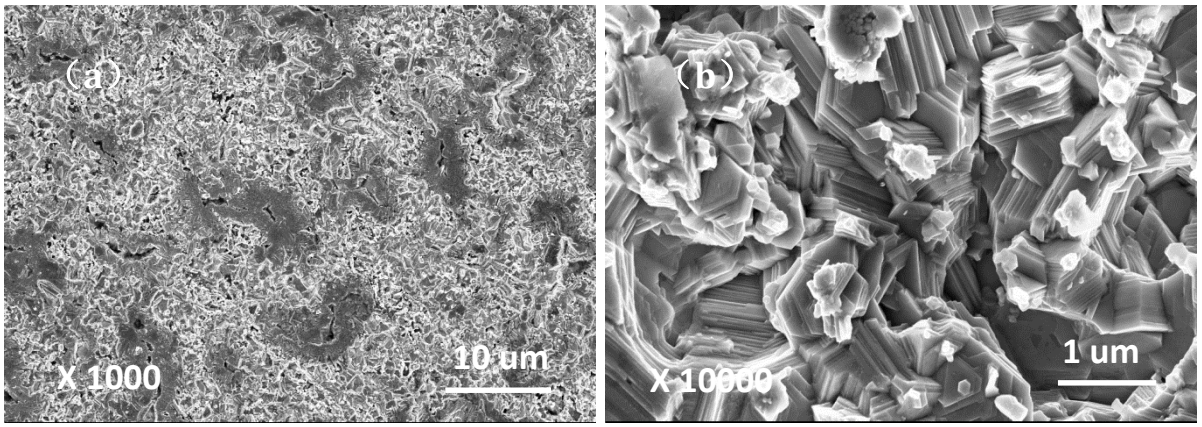

Figure 4.2 SEM image of Zn anode:
(a) TG#1 at X1000 magnification; (b) TG#1 at X10000 magnification.

4.2 Corrosion Test by Using Linear Polarization

Fig. 4.3 shows the Tafel plot result of commercial Zn and TG#1 respectively, while Tab. 4.1 gives the accurate parameter values. The corrosion current I_{corr} can be calculated from the measured polarization curve based on equations on Section 2.5.

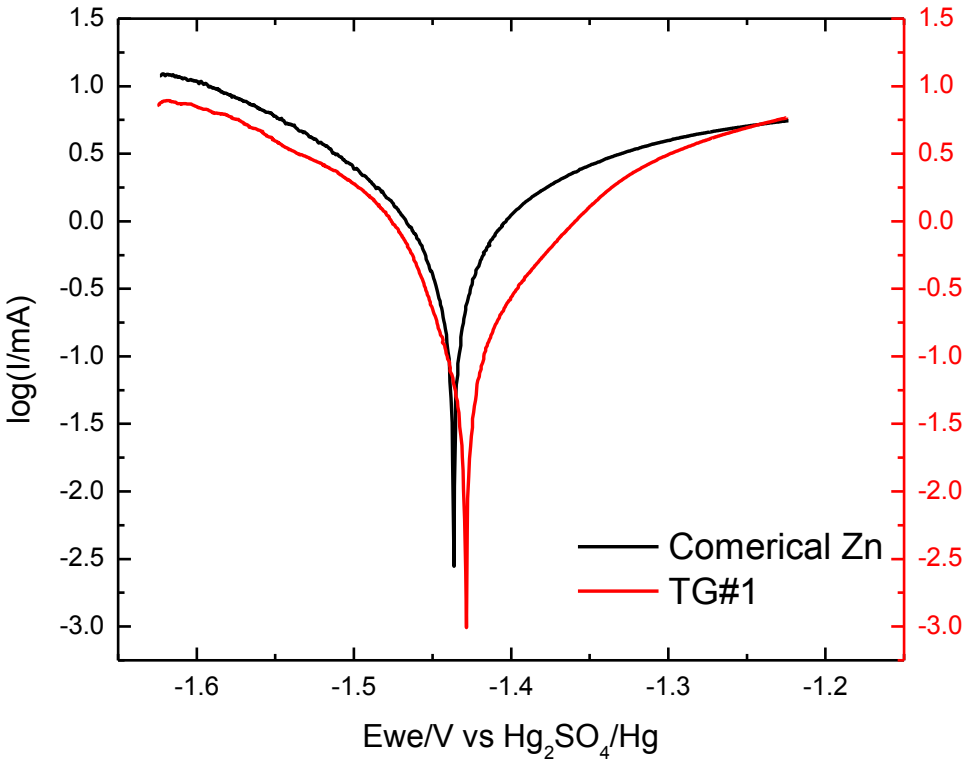

Figure 4.3 Tafel plot result of Zn anodes:

Black line on the top: Commercial Zn; Red line on the bottom: TG#1

From Table 4.1, the anode TG#1 has slightly higher corrosion potential and 46.81% less corrosion current comparing to characteristics of commercial Zn. The polarization resistance R_p can be calculated by the equation 3.1 and 3.2.

Substituting the values on Table 4.1, the polarization resistance of commercial Zn is 35.85 Ω, while the polarization resistance of TG#1 is 55.22 Ω. It means that the anode TG#1 has relatively better corrosion resistance.

Table 4.1 Comparison of Tafel fit results on commercial Zn and TG#1

	E_{corr}	I_{corr}	β_c	β_a
Commercial Zn	-1 436.570 mV	1 360.753 μA	180.2 mV	296.8 mV
TG#1	-1 429.395 mV	723.824 μA	163.0 mV	210.8 mV

4.3 Battery Cycle Performance and Electrochemical Impedance Spectroscopy (EIS)

4.3.1 Battery cycle performance

Battery cycle test has been carried on between commercial Zn and TG#1 for 300 cycles. After 200 and 300 cycles, battery capacity retention is recorded in order to qualitative evaluate battery performance, respectively. For each system, four parallel cells are tested under the same conditions to grasp their performance dispersion.

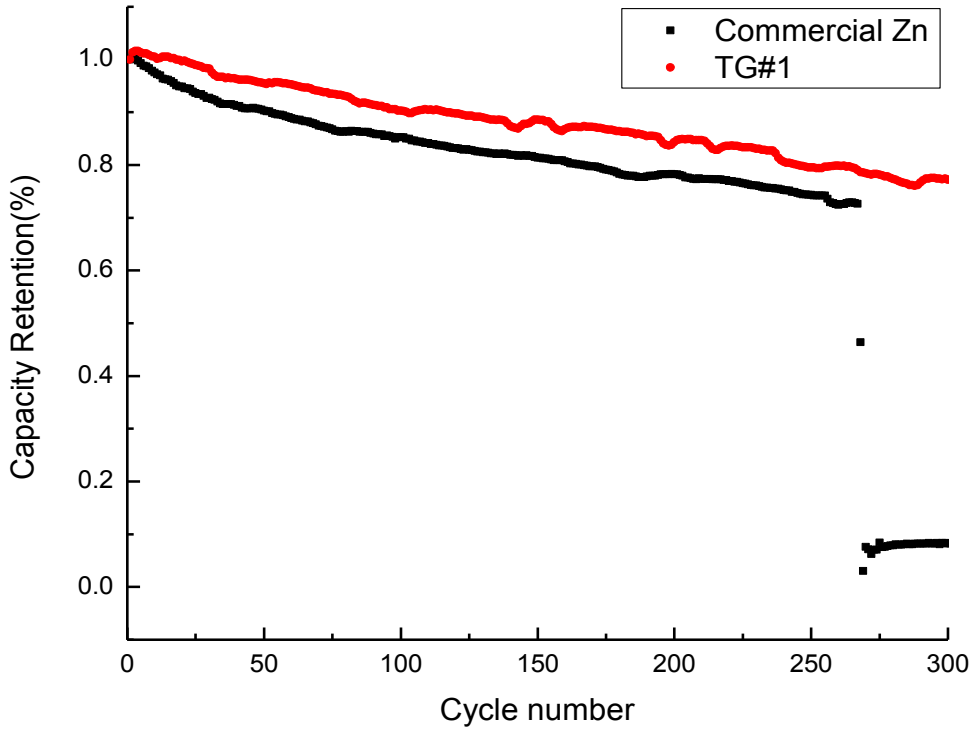

Figure 4.4 Galvanostatic charge/discharge cycle performance of ReHAB system with commercial Zn and TG#1 anodes.

As shown in Fig. 3.4, after 200 cycles running, batteries using commercial Zn anodes had capacity retention of 78.2%, yet batteries with TG#1 anodes had 84.3% capacity retention. While after 300 cycles running, batteries with TG#1 anodes had 77.2% capacity retention, yet batteries using commercial Zn anodes were all dead between 220-270 cycles. It means TG#1 was a relative better anode material on battery cycle.

4.3.2 Electrochemical Impedance Spectroscopy (EIS)

Electrochemical impedance profiles have been investigated on both commercial Zn and TG#1 after cycles running in the above section.

Fig. 4.5 displays the Nyquist plots of the EIS measurement for batteries using commercial Zn and TG#1 as anode after cycles.

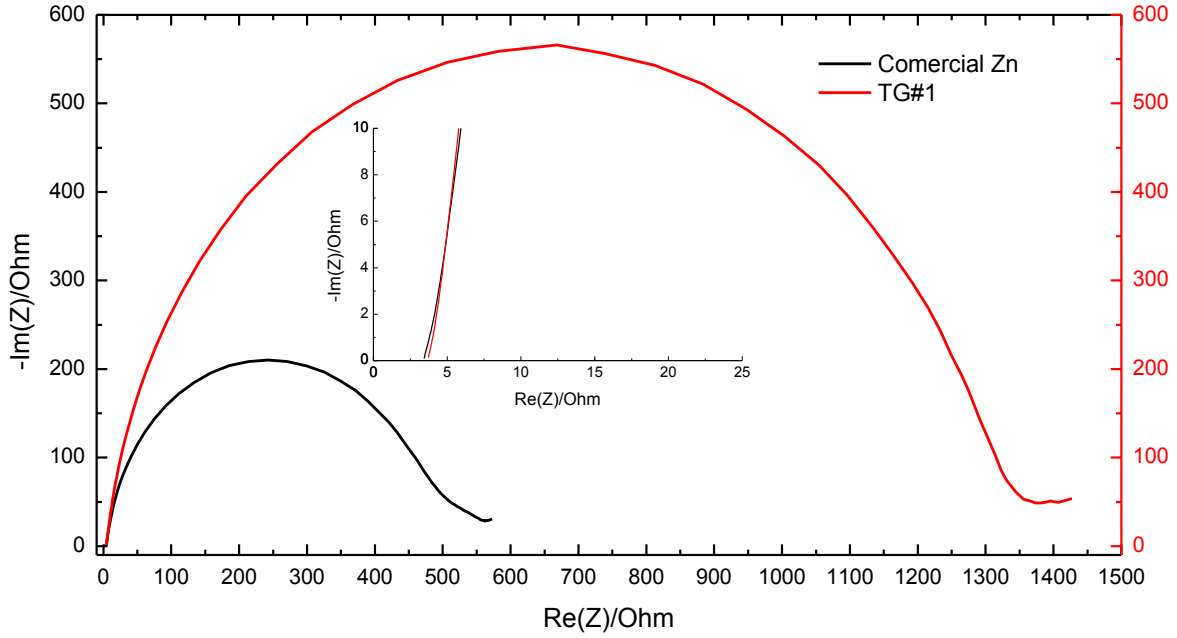

Figure 4.5 EIS profile of ReHAB anodes after 300 cycle test:

Black line on the bottom: Commercial Zn; Red line on the top: TG#1

Comparing two plots, it could be seen that the polarization resistances measured by EIS for commercial Zn and TG#1 had a same trend. It also could be seen that the battery with commercial Zn anode has lower polarization resistance than battery using TG#1 which means the former ones consumes less energy during charge-discharge process.

4.4 Float Charge Current and Elemental Analysis

4.4.1 Float Charge Current

Float charge current test has been carried on between commercial Zn and TG#1 at both room temperature (25 ℃) and high temperature (60 ℃). After float charge, float currents are recorded in order to qualitative evaluate on battery performance. Four parallel cells are tested under the same conditions to grasp their performance dispersion. Fig. 4.6 shows the result of float charge current at two temperatures between commercial Zn and TG#1.

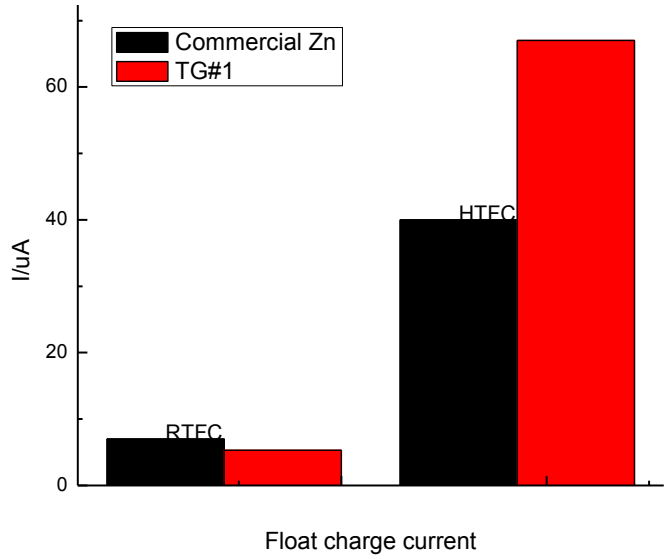

Figure 4.6 Float charge current on room temperature(RTFC) and high temperature(HTFC) for commercial Zn and TG#1

At room temperature (25 ℃), float charge current of commercial Zn is higher than that of TG#1 which means less side reactions happening in batteries using TG#1 anode. While at high temperature (60 ℃), float charge current of commercial Zn is less than of TG#1 which means less side reactions happened on batteries with commercial Zn anode. Batteries with TG#1 anodes exhibit better room temperature float charge performance, while batteries with commercial Zn anodes show significantly better high temperature float charge performance.

4.4.2 Elemental analysis

Elemental analysis has been conducted on cathodes of both commercial Zn and TG#1 anode batteries after float charge test in the above section. Carbon percentages on LMO cathode are recorded in order to qualitative evaluate on side reaction during float charge experiment.

Fig. 4.7 shows carbon percentages of cathode materials after both room temperature and high temperature float charge.

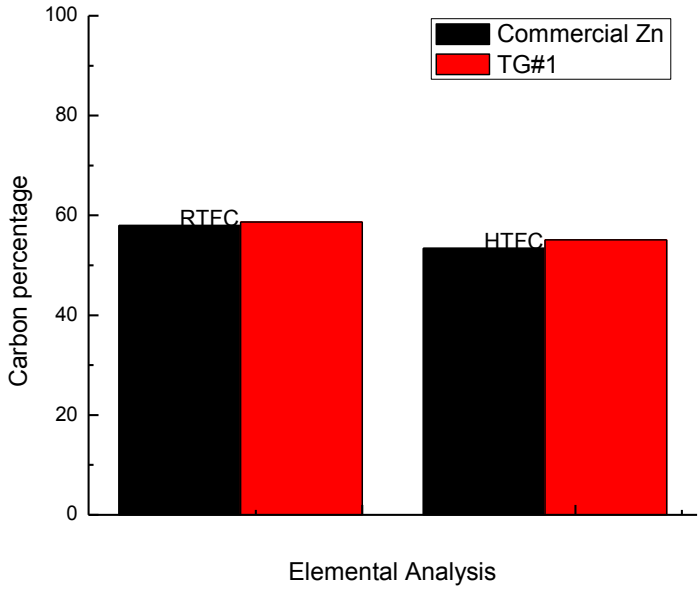

Figure 4.7 Carbon percentage of cathode material after float charge at room temperature(RTFC) and high temperature(HTFC) for commercial Zn and TG#1

Results indicate that batteries with TG#1 anode have more carbon on cathode materials after both RTFC and HTFC which suggest those with TG#1 anode are more stable on cathode material during float charge process.

4.5 Summary for TG#1 anode

4.5.1 Characterization of electrowinning Zn and Commercial Zn

The XRD pattern results indicate the electrowinning Zn with thiourea and gelatin as additives prefer to grow along certain direction. The different intensity of peaks also indicates different crystal orientation. The intensities of planes (100) and (002) on TG#1 are much higher, while the planes (101), (102), (200), (112), (201) all showed lower intensities compare to which of commercial Zn. SEM images suggest that on relatively lower magnification, TG#1 shows relatively uniform surface. On relatively higher magnification, the morphology of TG#1 could be characterized by the formation of fine-grained & porous deposits.

Since Zn are usually characterized by the formation of fine-grained, non-porous, ductile deposits when the crystal orientation is either random or the (101) orientation predominates and unsatisfactory conditions are usually associated with porous, brittle and coarse-grained deposits, in such cases the (110), (100), (211), and (112) crystal orientations predominate, the porous deposits might relate to the high intensity of plane (100) and fine-grained morphology is determined by lower intensities of various planes.

4.5.2 Electrochemical performance

The anode TG#1 has slightly higher corrosion potential and 46.81% less corrosion current compare to data of commercial Zn. It means that the anode TG#1 has the relative better corrosion resistance.

After 200 cycles, batteries using commercial Zn anodes had capacity retention of 78.2%, yet batteries with TG#1 anodes had 84.3% capacity retention. While after 300 cycles running, batteries with TG#1 anodes had 77.2% capacity retention, yet batteries using commercial Zn anodes were all dead between 220-270 cycles. It means TG#1 was a relative better anode material on battery cycle. While the polarization resistances measured by EIS for commercial Zn and TG#1 does not show the same trend.

At room temperature (25 ℃), float charge current of commercial Zn is higher than that of TG#1 which means less side reactions happening on batteries using TG#1 anode. While at high temperature (60 ℃), float charge current of commercial Zn is less than of TG#1 which means less side reactions happening on batteries using commercial Zn anode. Elemental analysis results indicate that batteries with TG#1 anode have more carbon on cathode materials after both RTFC and HTFC which suggest those with TG#1 anode are more stable on cathode material during float charge process.

Based on the results above, the advantages on battery performance of TG#1 anodes could be attributed to the porous and fine-grained deposits, preferable crystal orientations and high corrosion resistance. As the passivation of Zn has always been a problem for Zn related batteries [79-81], the porous surface could highly inhibit Zn passivation process by increase surface area (active material) during battery cycle test. The fine-grained deposits provide relatively uniform current distribution that could contribute to lower float charge current.

Chapter 5

Performance of Electro-winning Zinc ITG#1 on ReHAB

The Effect of In and thiourea on electrochemical properties of Zn is investigated in this chapter. 30mg/L $In_2(SO_4)_3$, 30mg/L thiourea and 10mg/L gelatin has been added into the eletrowinning electrolyte during process 2.1. Preliminary experiments show that In could not obtain success eletrowinning without adding other additives. So organic additive thiourea has been introduced into this experiment. The range of 5 mg/L to 100 mg/L In has been tested. The best electrochemical results were obtained at the range of 20 mg/L to 40 mg/L In with 30mg/L thiourea. Considering both industrial costs and comparability, total amount of 30mg/L In and 30 mg/L thiourea have been added in the experiment. All results are compared with those of commercial Zn.

5.1 XRD & SEM test on Electro-winning Zn ITG#1

5.1.1 XRD Results

The XRD patterns of both commercial Zn and ITG#1 have been compared on Fig.5.1.

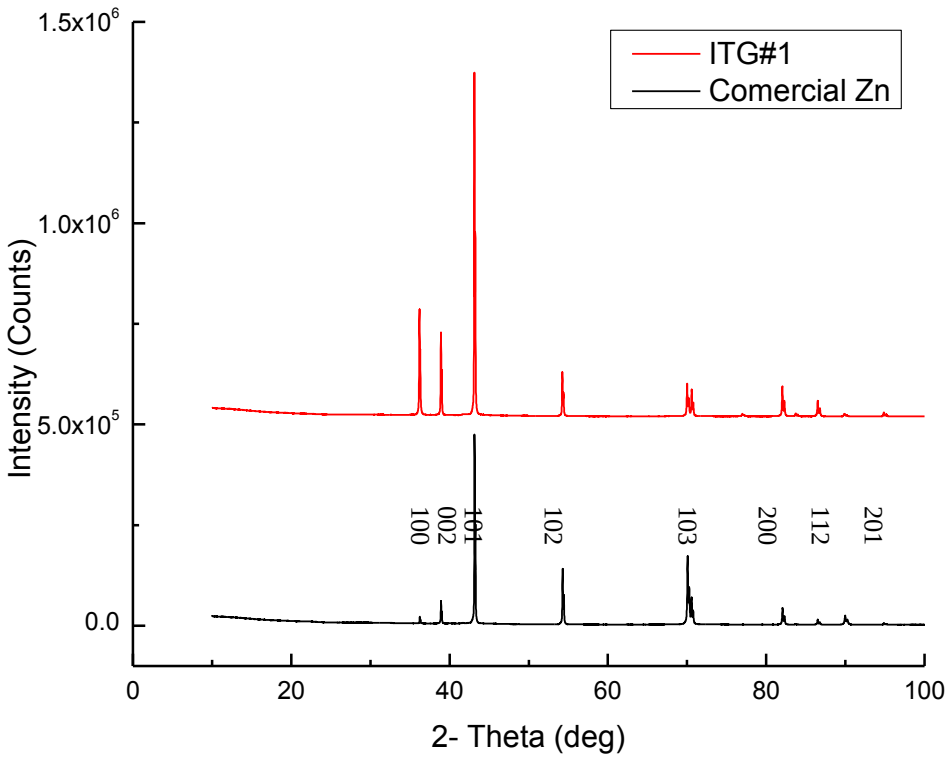

Figure 5.1 Comparison of XRD pattern :

Red plot on the top: ITG#1 anode; Black plot on the bottom: Commercial Zn anode.

From the above XRD pattern, it could be observed that both samples are pure Zn. However, different with commercial Zn, the intensities of planes (100) (002) and (101) on ITG#1 are much higher, while planes (200), (112), (201) showed lower intensity. Other crystal orientation changes are observed that in which the plane (102) showed similar intensities.

The results indicate the electrowinning Zn with thiourea, In and gelatin as additives prefers to grow along certain directions. The different intensity of peaks also indicated

different crystal orientation.

5.1.2 SEM Test Results

SEM images with different magnification are shown in Fig. 5.2. Comparing to commercial Zn on Fig. 3.2(a)&(b), on relatively lower magnification, the morphology of ITG#1 shows relative uniform surface on X1000 magnification. On relatively higher magnification, the morphology of ITG#1 is a mixed basal type[31] and characterized by the formation of coarse-grained & porous, while commercial Zn does not show any deposition type. The porous deposits might relate to the high intensities of planes (100) and (002). ITG#1 shows similar morphology as TG#1, but the former one is has finer surface and more porous.

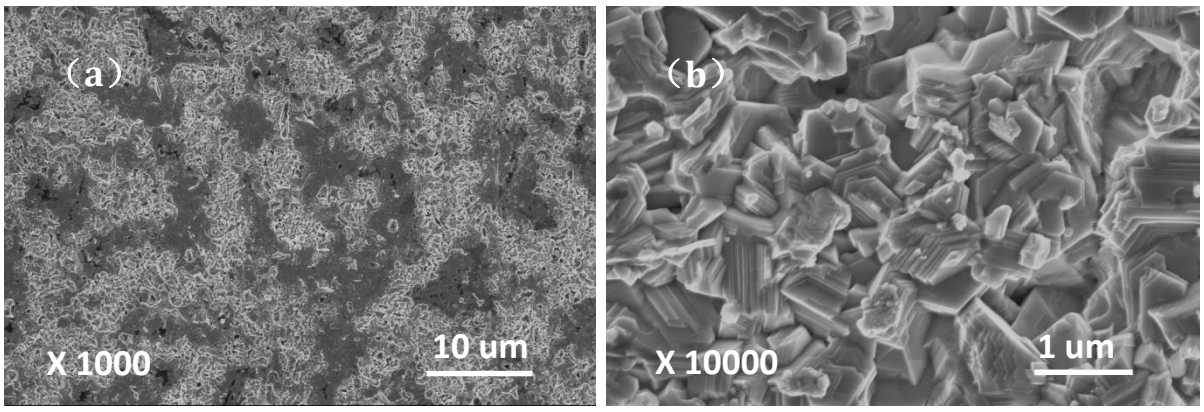

Figure 4.2 SEM image of Zn anode:
(a) ITG#1 at X1000 magnification; (b) ITG#1 at X10000 magnification.

5.2 Corrosion Test by Using Linear Polarization

Fig. 5.3 shows the Tafel plot result of commercial Zn and ITG#1 respectively, while Tab. 5.1 gives accurate parameter values. The corrosion current I_{corr} can be calculated from the measured polarization curve based on equations on Section 2.5.

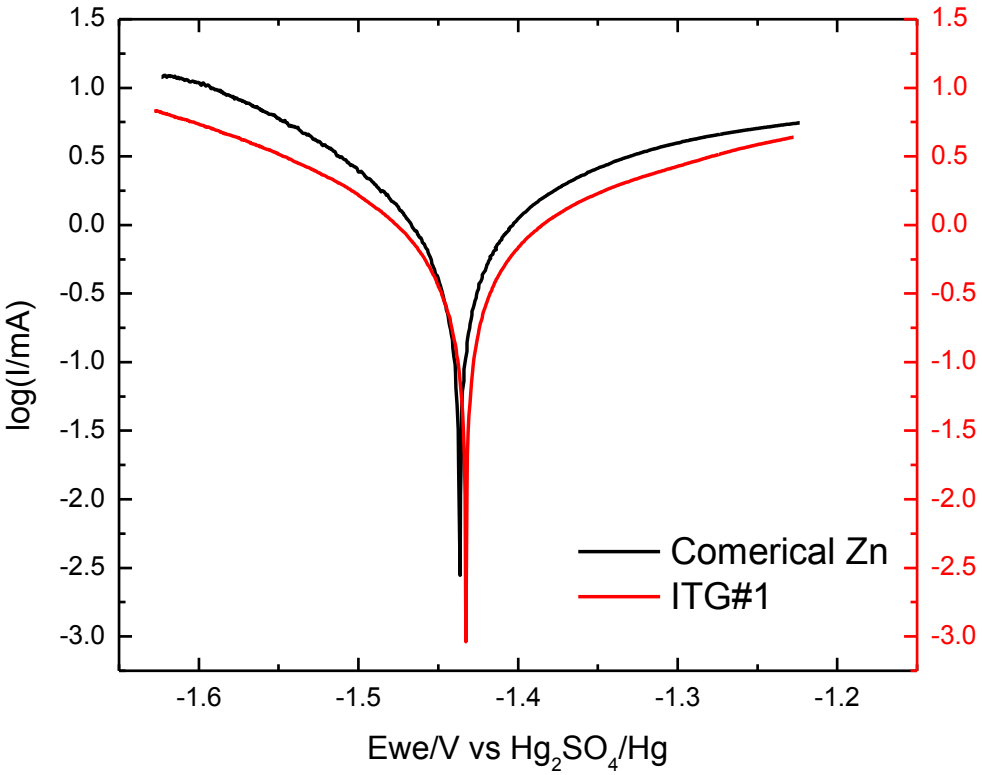

Figure 5.3 Tafel plot result of Zn anodes:

Black line on the top: Commercial Zn; Red line on the bottom: ITG#1

From Table 5.1, the anode ITG#1 has slightly higher corrosion potential and 31.10% less corrosion current comparing to characteristics of commercial Zn. The polarization resistance R_p can be calculated by the equation 3.1 and 3.2.

Substituting the values on Table 5.1, the polarization resistance of commercial Zn is 35.85 Ω, while the polarization resistance of ITG#1 is 58.51 Ω. It means that the anode ITG#1 has relatively better corrosion resistance.

Table 5.1 Comparison of Tafel fit results on commercial Zn and ITG#1

	E_{corr}	I_{corr}	β_c	β_a
Commercial Zn	-1 436.570 mV	1 360.753 μA	180.2 mV	296.8 mV
ITG#1	-1 432.203 mV	937.592 μA	220.5 mV	295.0 mV

5.3 Battery Cycle Performance and Electrochemical Impedance Spectroscopy (EIS)

5.3.1 Battery cycle performance

Battery cycle test has been carried on between commercial Zn and ITG#1 for 300 cycles. After 200 and 300 cycles, battery capacity retention is recorded in order to qualitative evaluate battery performance, respectively. Four parallel cells are tested under the same conditions to grasp their performance dispersion.

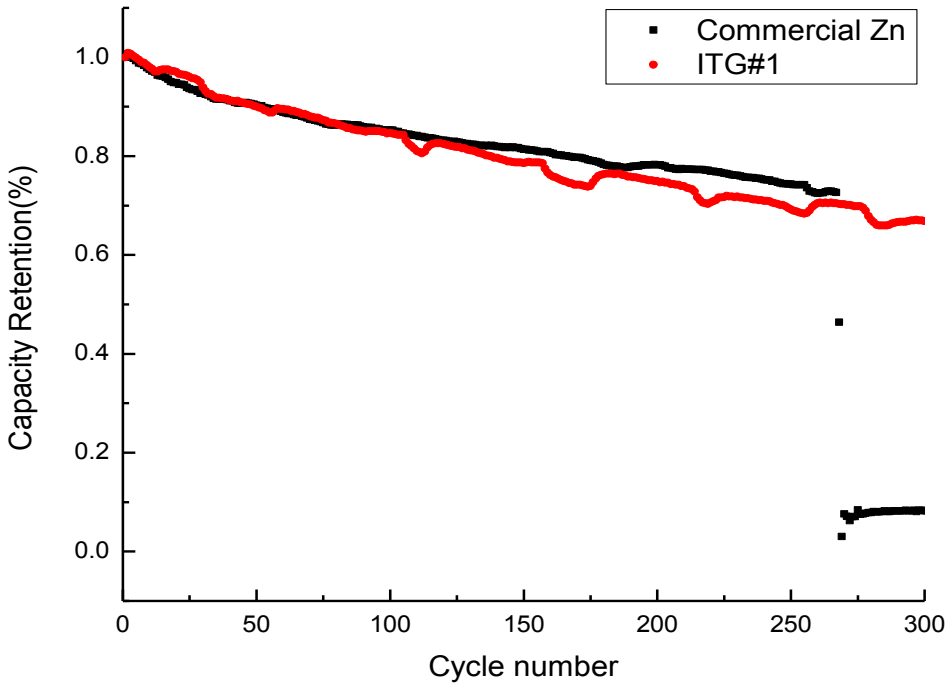

Figure 5.4 Galvanostatic charge/discharge cycle performance of ReHAB system with commercial Zn and ITG#1 anodes.

As shown in Fig. 3.4, after 200 cycles running, batteries using anodes had capacity retention of 78.2%, yet batteries with ITG#1 anodes had 75.0% capacity retention. While after 300 cycles running, batteries with ITG#1 anodes had 66.9% capacity retention, yet batteries using commercial Zn anodes were all dead between 220-270 cycles. It means commercial Zn was a relative better anode material before 200 cycles, but batteries with ITG#1 anodes shows more stable cycle performance.

5.3.2 Electrochemical Impedance Spectroscopy (EIS)

Electrochemical impedance profiles have been investigated on both commercial Zn and ITG#1 after cycles running in the above section.

Fig. 5.5 displays the Nyquist plots of the EIS measurement for batteries using commercial Zn and ITG#1 as anode after cycles.

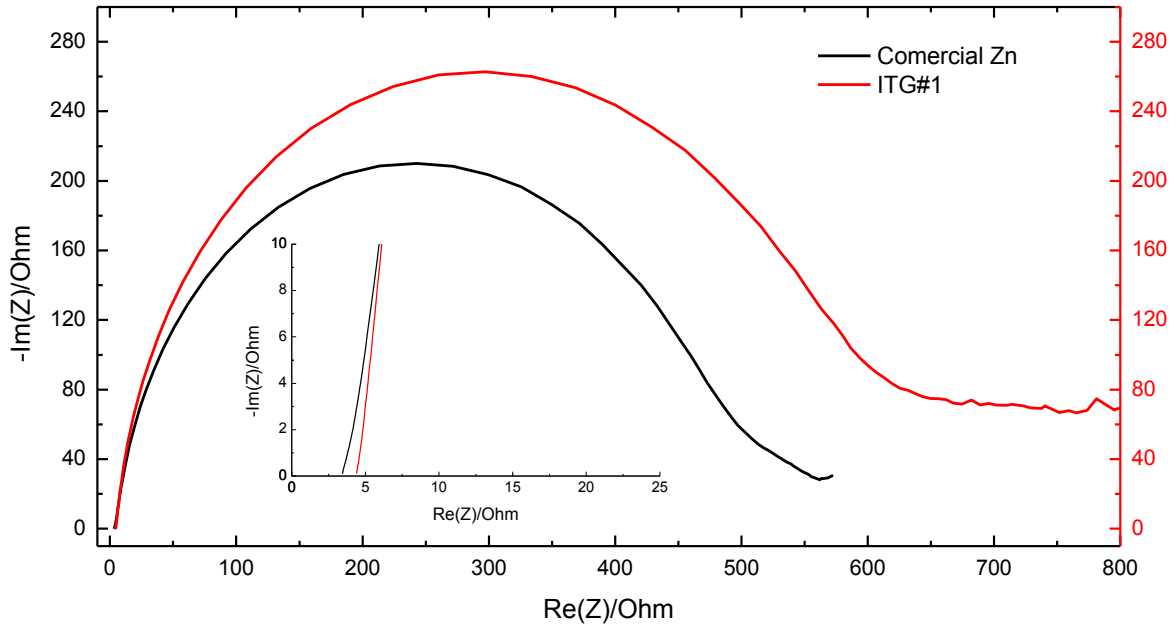

Figure 5.5 EIS profile of ReHAB anodes after 200 cycle test:

Black line on the bottom: Commercial Zn; Red line on the top: ITG#1

Comparing two plots, it could be seen that the polarization resistances measured by EIS for commercial Zn and ITG#1 had a same trend. It also could be seen that the battery with commercial Zn anode has lower polarization resistance than battery using ITG#1 anode which means the former ones consumes less energy during charge-discharge process.

5.4 Float Charge Current and Elemental Analysis

5.4.1 Float Charge Current

Float charge current test has been carried on between commercial Zn and ITG#1 at both room temperature (25 ℃) and high temperature (60 ℃). After float charging, float currents are recorded in order to qualitative evaluate on battery performance. Four parallel cells are tested under the same conditions to grasp their performance dispersion. Fig. 5.6 shows the result of float charge current at two temperatures between commercial Zn and ITG#1.

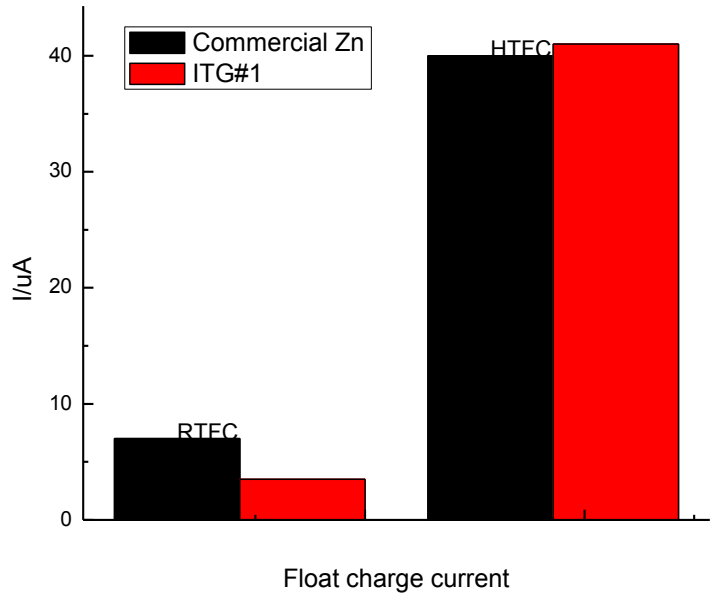

Figure 5.6 Float charge current on room temperature(RTFC) and high temperature(HTFC) for commercial Zn and ITG#1

At room temperature (25 ℃), float charge current of commercial Zn is more than that twice of ITG#1 which means less side reactions happening in batteries using ITG#1 anode. While at high temperature (60 ℃), float charge current of commercial Zn is slightly less than of ITG#1 which means less side reactions happened on batteries with commercial Zn anode. Batteries with ITG#1 anodes exhibit significantly better room temperature

float charge performance, while batteries with commercial Zn anodes show slightly better high temperature float charge performance.

5.4.2 Elemental analysis

Elemental analysis has been conducted on cathodes of both commercial Zn and ITG#1 anode batteries after float charge test in the above section. Carbon percentages on LMO cathode are recorded in order to qualitative evaluate on side reaction during float charge experiment.

Fig. 5.7 shows carbon percentages of cathode materials after both room temperature and high temperature float charge.

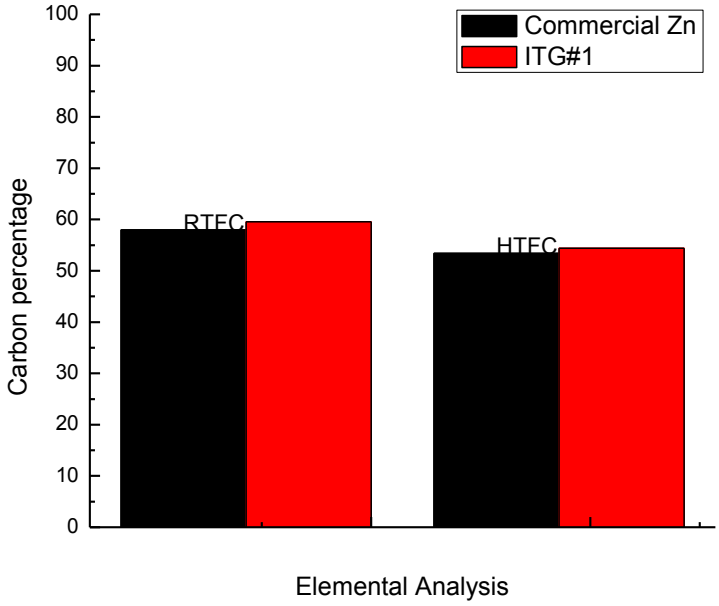

Figure 5.7 Carbon percentage of cathode material after float charge at room temperature(RTFC) and high temperature(HTFC) for commercial Zn and ITG#1

Results indicate that batteries with ITG#1 anode have more carbon on cathode materials after both RTFC and HTFC which suggest those with ITG#1 anode are more stable on cathode material during float charge process.

5.5 Summary for ITG#1 anode

5.5.1 Characterization of electrowinning Zn and Commercial Zn

XRD pattern results indicate the electrowinning Zn with thiourea, In and gelatin as additives prefer to grow along certain direction. The different intensity of peaks also indicate different crystal orientation. The intensities of planes (100) (002) and (101) on ITG#1 are much higher, while planes (200), (112), (201) showed lower intensity. Other crystal orientation changes are observed that in which the plane (102) showed similar intensities. SEM images suggest that on relatively lower magnification, ITG#1 shows relative uniform surface. On relatively higher magnification, the morphology of ITG#1 could be characterized by the formation of coarse-grained & porous, while commercial Zn does not show any deposition type.

The porous deposits might relate to the high intensities of planes (100) and (002). ITG#1 shows similar morphology as TG#1, but the latter one is more porous and has finer surface.

5.5.2 Electrochemical performance

The anode ITG#1 has slightly higher corrosion potential and 31.10% less corrosion current compare to data of commercial Zn. It means that the anode ITG#1 has the relative better corrosion resistance.

After 200 cycles, batteries using anodes had capacity retention of 78.2%, yet batteries with ITG#1 anodes had 75.0% capacity retention. While after 300 cycles running, batteries with ITG#1 anodes had 66.9% capacity retention, yet batteries using commercial Zn anodes were all dead between 220-270 cycles. It means commercial Zn was a relative better anode material before 200 cycles, but batteries with ITG#1 anodes shows more stable cycle performance. The polarization resistances measured by EIS for commercial Zn and ITG#1 have the same trend. It also could be seen that the battery with commercial Zn anode has lower polarization resistance than ITG#1 which means the

former ones consumes less energy during charge-discharge process.

At room temperature (25 ℃), float charge current of commercial Zn is more than twice that of ITG#1 which means less side reactions happening on batteries using ITG#1 anode. While at high temperature (60 ℃), float charge current of commercial Zn is slightly less than of ITG#1 which means less side reactions happening on batteries using commercial Zn anode. Elemental analysis results indicate that batteries with ITG#1 anode have more carbon on cathode materials after both RTFC and HTFC which suggest those with ITG#1 anode are more stable on cathode material during float charge process.

Chapter 6

Performance of Electro-winning Zinc hBITG#1 on ReHAB

The Effect of Bi, In and thiourea on electrochemical properties of Zn is investigated in this chapter. Considering both industrial costs and comparability, 15mg/L Bi_2O_3, 15mg/L $In_2(SO_4)_3$, 30mg/L thiourea and 10mg/L gelatin has been added into the eletrowinning electrolyte during process 2.1. All results are compared with those of commercial Zn.

6.1 XRD&SEM test on Electro-winning Zn hBITG#1

6.1.1 XRD Results

The XRD patterns of both commercial Zn and hBITG#1 have been compared on Fig.6.1.

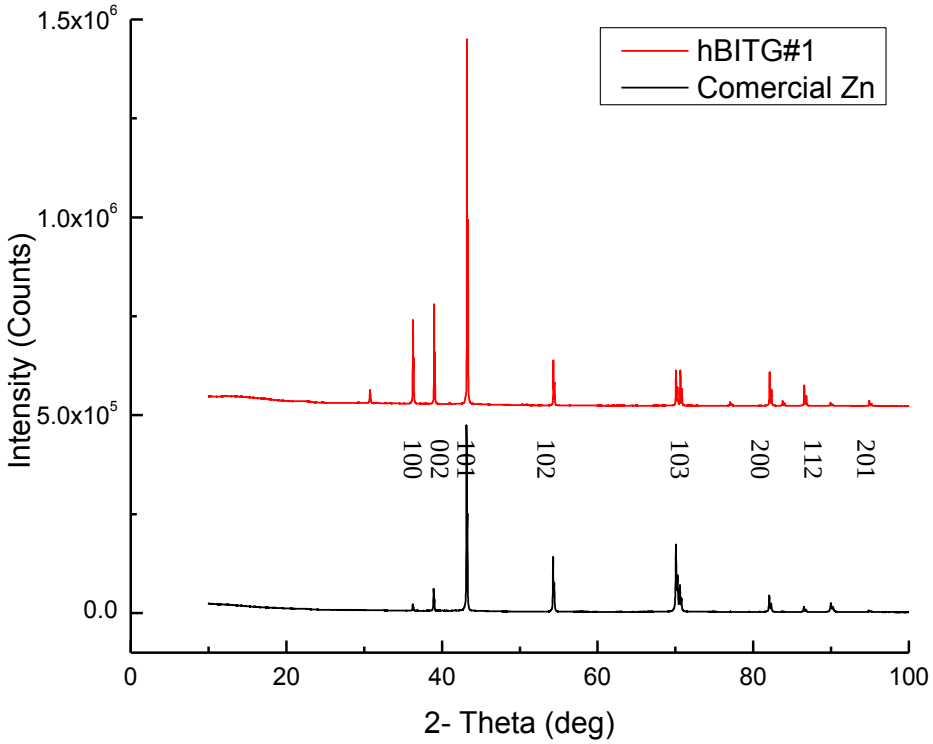

Figure 6.1 Comparison of XRD pattern:

Red plot on the top: hBITG#1 anode; Black plot on the bottom: Commercial Zn anode.

From the above XRD pattern, it could be observed that both samples are pure Zn. However, different with commercial Zn, the intensities of plane (100), (002), (101), (200), (112) on hBITG#1 is much higher, while planes (103), (201) all show lower intensities. Other crystal orientation changes are observed that in which the plane (102) shows similar intensity.

The results indicate the electrowinning Zn with thiourea, In, Bi and gelatin as additives prefers to grow along certain directions. The different intensity of peaks also indicated different crystal orientation.

6.1.2 SEM Test Results

SEM images with different magnification are shown in Fig. 6.2. Comparing to commercial Zn on Fig. 3.2(a)&(b), on relative lower magnification, the morphology of hBITG#1 shows

relative uniform surface on X1000 magnification. On relatively higher magnification, the morphology of hBITG#1 is an incomplete basal type[31] and characterized by the formation of coarse-grained & porous. The porous deposits might relate to the high intensity of plane (100), while coarse-grained morphology is determined by higher intensities of various planes, except plane (101). The morphology of hBITG#1 is similar with both TG#1 and ITG#1, but shows a less uniform surface and larger deposits.

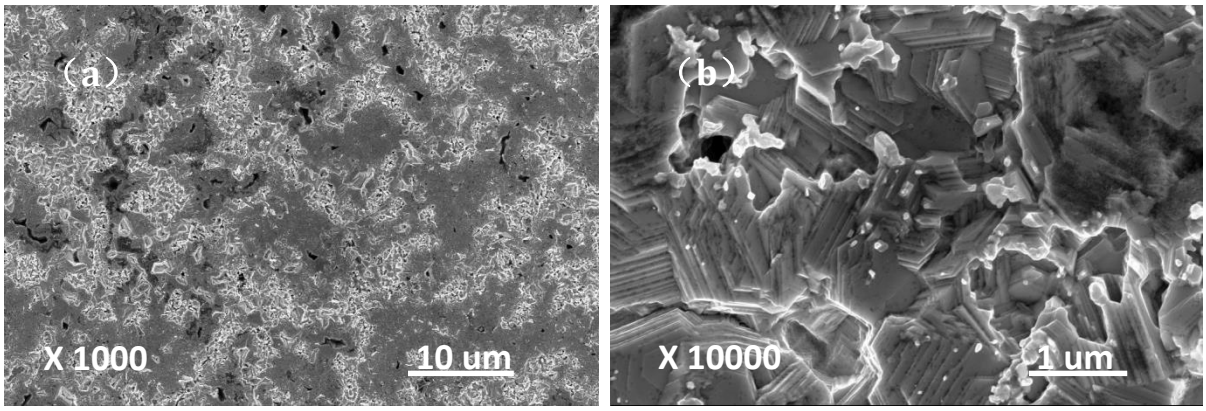

Figure 6.2 SEM image of Zn anode:
(a) hBITG#1 at X1000 magnification; (b) hBITG#1 at X10000 magnification.

6.2 Corrosion Test by Using Linear Polarization

Fig. 6.3 shows the Tafel plot result of commercial Zn and hBITG#1 respectively, while Tab. 6.1 gives accurate parameter values. The corrosion current I_{corr} can be calculated from the measured polarization curve based on equations on Section 2.5.

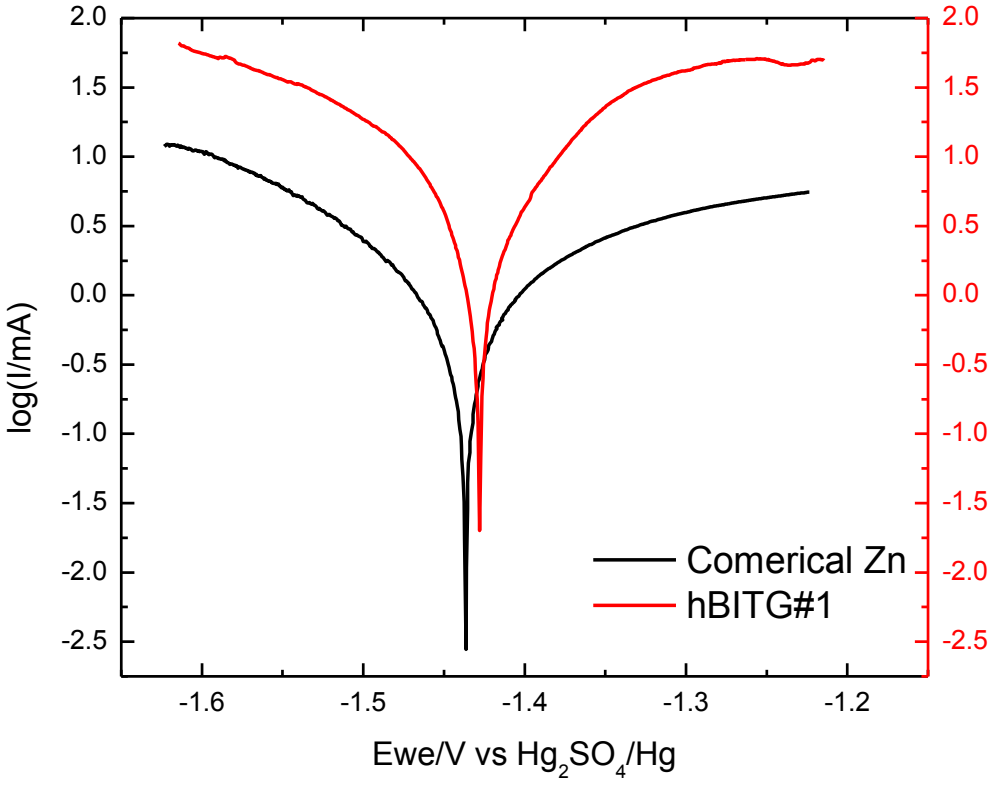

Figure 6.3 Tafel plot result of Zn anodes:

Black line on the bottom: Commercial Zn; Red line on the top: hBITG#1

From Table 6.1, the anode hBITG#1 has similar corrosion potential and almost 6.6 times higher corrosion current comparing to commercial Zn. The polarization resistance R_p can be calculated by the equation 3.1 and 3.2.

Substituting the values on Table 6.1, the polarization resistance of commercial Zn is 35.85 Ω, while the polarization resistance of hBITG#1 is 4.61 Ω. It means that the anode hBITG#1 has significant worse corrosion resistance.

Table 6.1 Comparison of Tafel fit results on commercial Zn and hBITG#1

	E_{corr}	I_{corr}	β_c	β_a
Commercial Zn	-1 436.570 mV	1 360.753 µA	180.2 mV	296.8 mV
hBITG#1	-1 427.145 mV	9 052.225 µA	204.8 mV	180.3 mV

6.3 Battery Cycle Performance and Electrochemical Impedance Spectroscopy (EIS)

6.3.1 Battery cycle performance

Battery cycle test has been carried on between commercial Zn and TG#1 for 300 cycles. After 200 and 300 cycles, battery capacity retention is recorded in order to qualitative evaluate battery performance, respectively. For each system, four parallel cells are tested under the same conditions to grasp their performance dispersion.

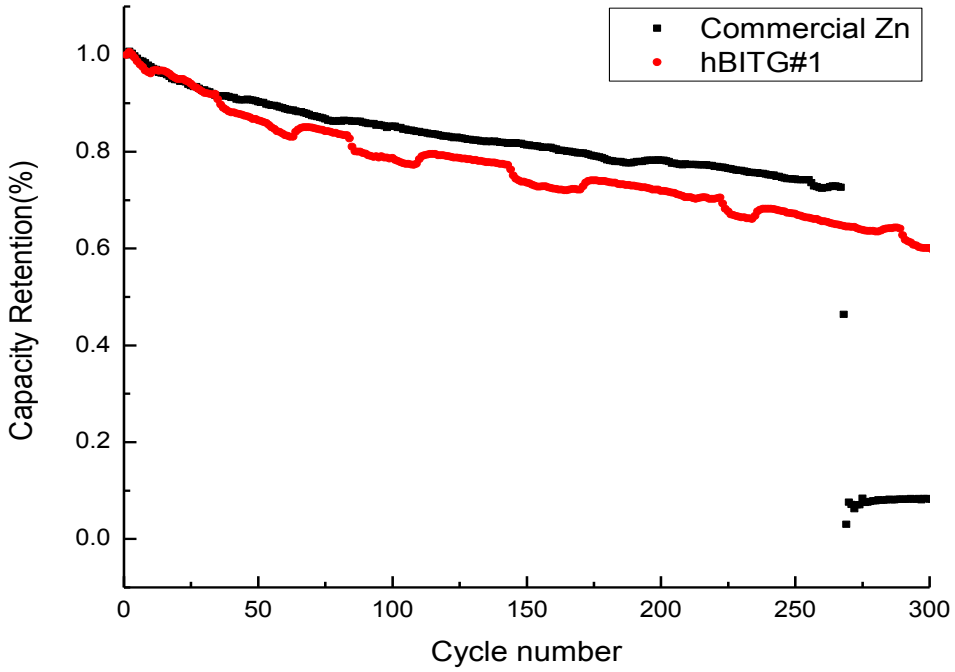

Figure 6.4 Galvanostatic charge/discharge cycle performance of ReHAB system with commercial Zn and hBITG#1 anodes.

As shown in Fig. 3.4, after 200 cycles running, batteries using anodes had capacity retention of 78.2%, yet batteries with hBITG#1 anodes had 71.9% capacity retention. While after 300 cycles running, batteries with hBITG#1 anodes had 59.8% capacity retention, yet batteries using commercial Zn anodes were all dead between 220-270 cycles. It means commercial Zn was a relative better anode material before 200 cycles, but batteries with hBITG#1 anodes shows more stable cycle performance.

6.3.2 Electrochemical Impedance Spectroscopy (EIS)

Electrochemical impedance profiles have been investigated on both commercial Zn and hBITG#1 after cycles running in the above section.

Fig. 6.5 displays the Nyquist plots of the EIS measurement for batteries using commercial Zn and hBITG#1 as anode after cycles.

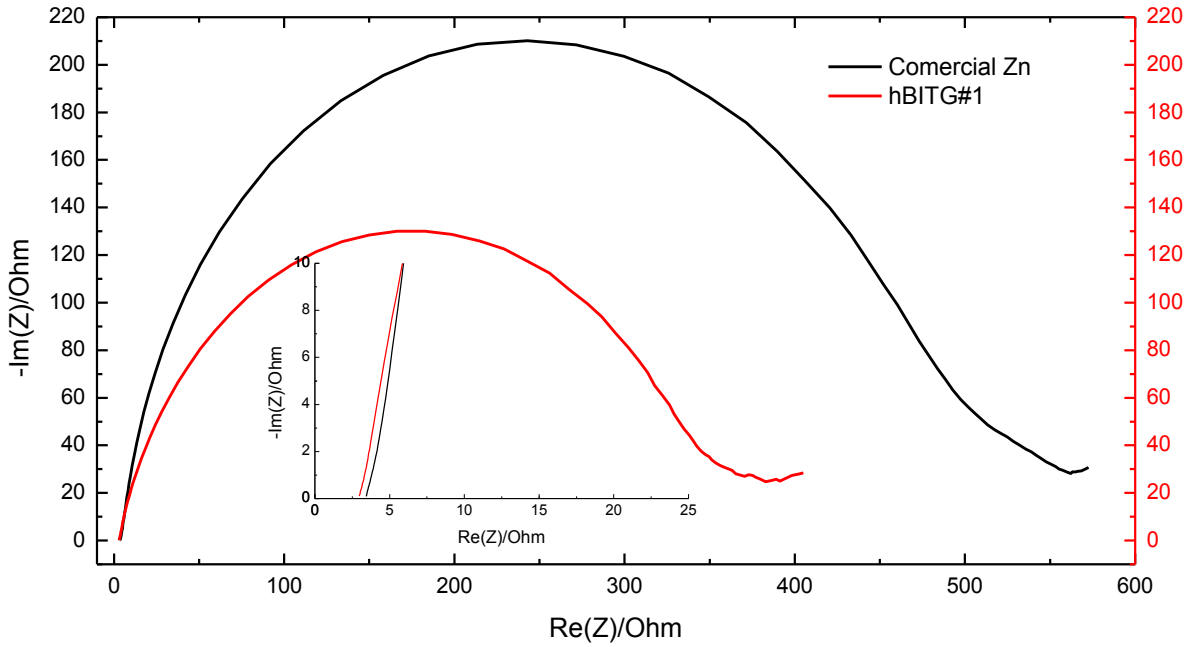

Figure 6.5 EIS profile of ReHAB anodes after 300 cycle test:

Black line on the top: Commercial Zn; Red line on the bottom: hBITG#1

Comparing two plots, it could be seen that the polarization resistances measured by EIS for commercial Zn and hBITG#1 had a same trend. It also could be seen that the battery with commercial Zn anode has higher polarization resistance than battery using hBITG#1 which means the former ones consumes more energy during charge-discharge process.

6.4 Float Charge Current and Elemental Analysis

6.4.1 Float Charge Current

Float charge current test has been carried on between commercial Zn and hBITG#1 at both room temperature (25 ℃) and high temperature (60 ℃). After float charging, float currents are recorded in order to qualitative evaluate on battery performance. Four parallel cells are tested under the same conditions to grasp their performance dispersion. Fig. 6.6 shows the result of float charge current at two temperatures between commercial Zn and hBITG#1.

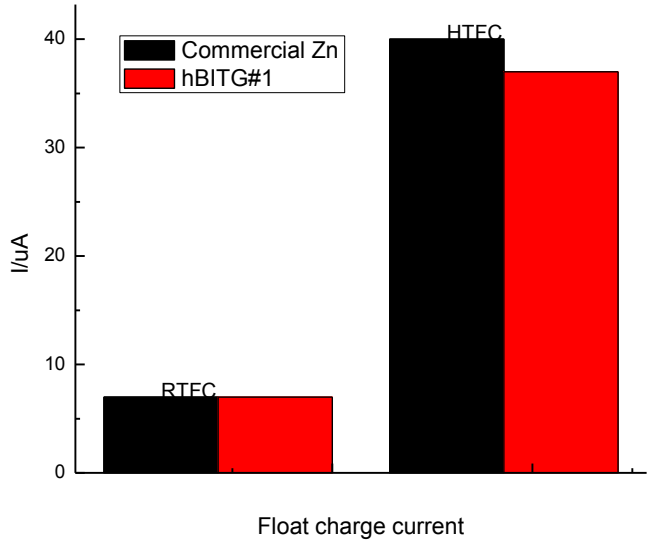

Figure 6.6 Float charge current on room temperature (RTFC) and high temperature (HTFC) for commercial Zn and hBITG#1

At room temperature (25 ℃), float charge current of commercial Zn is almost same as that of hBITG#1 which means side reactions happening on batteries does not have too much difference. While at high temperature (60 ℃), float charge current of commercial Zn is higher than of hBTG#1 which means less side reactions happened on batteries with hBTG#1 anode. Batteries with hBITG#1 anodes exhibit almost the same room

temperature float charge performance as which with commercial Zn anodes, while show better high temperature float charge performance.

6.4.2 Elemental analysis

Elemental analysis has been conducted on cathodes of both commercial Zn and hBITG#1 anode batteries after float charge test in the above section. Carbon percentages on LMO cathode are recorded in order to qualitative evaluate on side reaction during float charge experiment.

Fig. 6.7 shows carbon percentages of cathode materials after both room temperature and high temperature float charge.

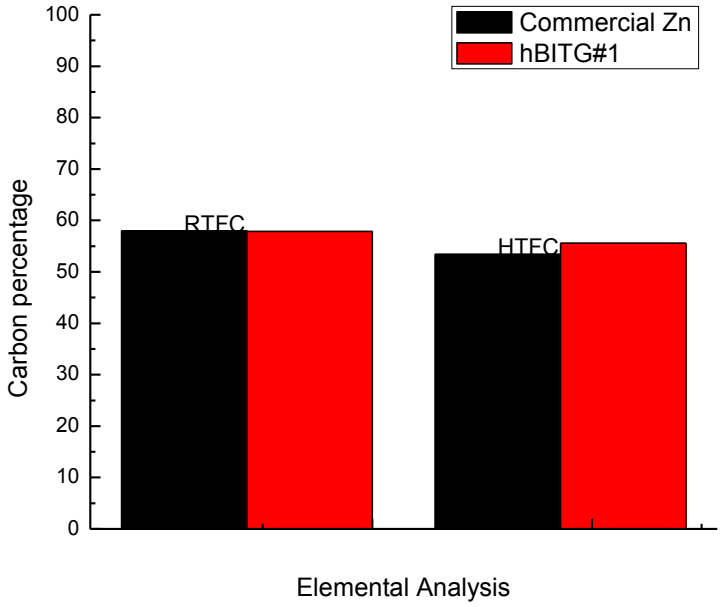

Figure 6.7 Carbon percentage of cathode material after float charge at room temperature(RTFC) and high temperature(HTFC) for commercial Zn and hBITG#1

Results indicated that batteries with hBITG#1 anode have more carbon on cathode materials after both RTFC and HTFC which suggest those with hBITG#1 anode are more stable on cathode material during float charge process.

6.5 Summary for hBITG#1 anode

6.5.1 Characterization of electrowinning Zn and Commercial Zn

XRD pattern results indicate the electrowinning Zn with thiourea, In, Bi and gelatin as additives prefer to grow along certain direction. The different intensity of peaks also indicates different crystal orientation. The intensities of plane (100), (002), (101), (200), (112) on hBITG#1 is much higher, while planes (103), (201) all show lower intensities. Other crystal orientation changes are observed that in which the plane (102) shows similar intensity. SEM images on relatively lower magnification, hBITG#1 anode showed relatively uniform surface. On relatively higher magnification, the morphology of hBITG#1 could be characterized by the formation of coarse-grained & porous.

The porous deposits might relate to the high intensity of plane (100), while coarse-grained morphology is determined by higher intensities of various planes, except plane (101). The morphology of hBITG#1 is similar with both TG#1 and ITG#1, but shows a less uniform surface and larger deposits.

6.5.2 Electrochemical performance

The anode hBITG#1 has similar corrosion potential and almost 6.6 times corrosion current compare to data of commercial Zn. It meant that the anode hBITG#1 has significant worse corrosion resistance.

After 200 cycles, batteries using anodes had capacity retention of 78.2%, yet batteries with hBITG#1 anodes had 71.9% capacity retention. While after 300 cycles running, batteries with hBITG#1 anodes had 59.8% capacity retention, yet batteries using commercial Zn anodes were all dead between 220-270 cycles. It means commercial Zn was a relative better anode material before 200 cycles, but batteries with hBITG#1 anodes shows more stable cycle performance. The polarization resistances measured by EIS for commercial Zn and hBITG#1 do not show the same trend.

At room temperature (25 ℃), float charge current of commercial Zn is almost same

as that of hBITG#1 which means side reactions happening on batteries does not have too much difference. While at high temperature (60 ℃), float charge current of commercial Zn is higher than of hBTG#1 which means less side reactions happening on batteries using hBTG#1 anode. Elemental analysis results indicated that batteries with hBITG#1 anode have more carbon on cathode material after both RTFC and HTFC which suggest those with hBITG#1 anode are more stable on cathode material during float charge process.

Chapter 7

Conclusions and Recommendations

7.1 Conclusions

7.1.1 XRD & SEM test on Zn anodes

The XRD pattern results which show on Fig. 7.1 indicated the electrowinning Zn with different additives prefers to grow along different certain direction. The different intensity of peaks indicated different crystal orientation.

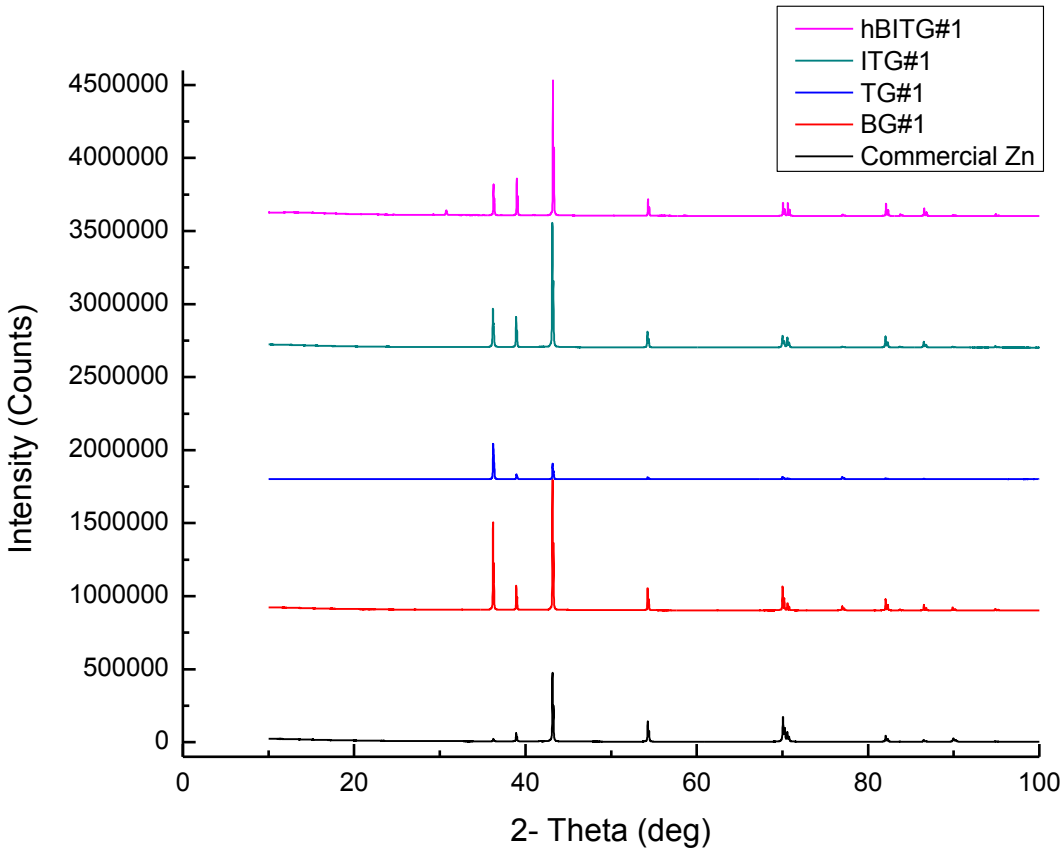

Figure 7.1 XRD pattern of Zn anodes

From the above XRD pattern, it could be observed that BG#1 has the highest intensity of (100), followed by ITG#1, TG#1, hBITG#1 and commercial Zn. And hBITG#1 has the highest intensity of (101), followed by ITG#1, BG#1, commercial Zn and hBITG#1. The results are corresponding to the morphologies observed on SEM tests.

SEM images on relative lower magnification, commercial Zn showed cutting marks which might be caused by the cutting process with manufacturer. All electrowinning anodes showed relative uniform surface on X1000 magnification. On relative higher magnification, the morphology of BG#1 is characterized by the formation of flat hexagonal & non-porous deposits, TG#1 is characterized by the formation of fine-grained & porous deposits, ITG#1 has relatively medium grain size & porous and hBITG#1 is characterized by the formation of coarse-grained & porous. While commercial Zn do not

show any deposition type. The morphology of electrowinning Zn is corresponded to its planes intensities. SEM images with different magnification are shown in Fig. 7.2.

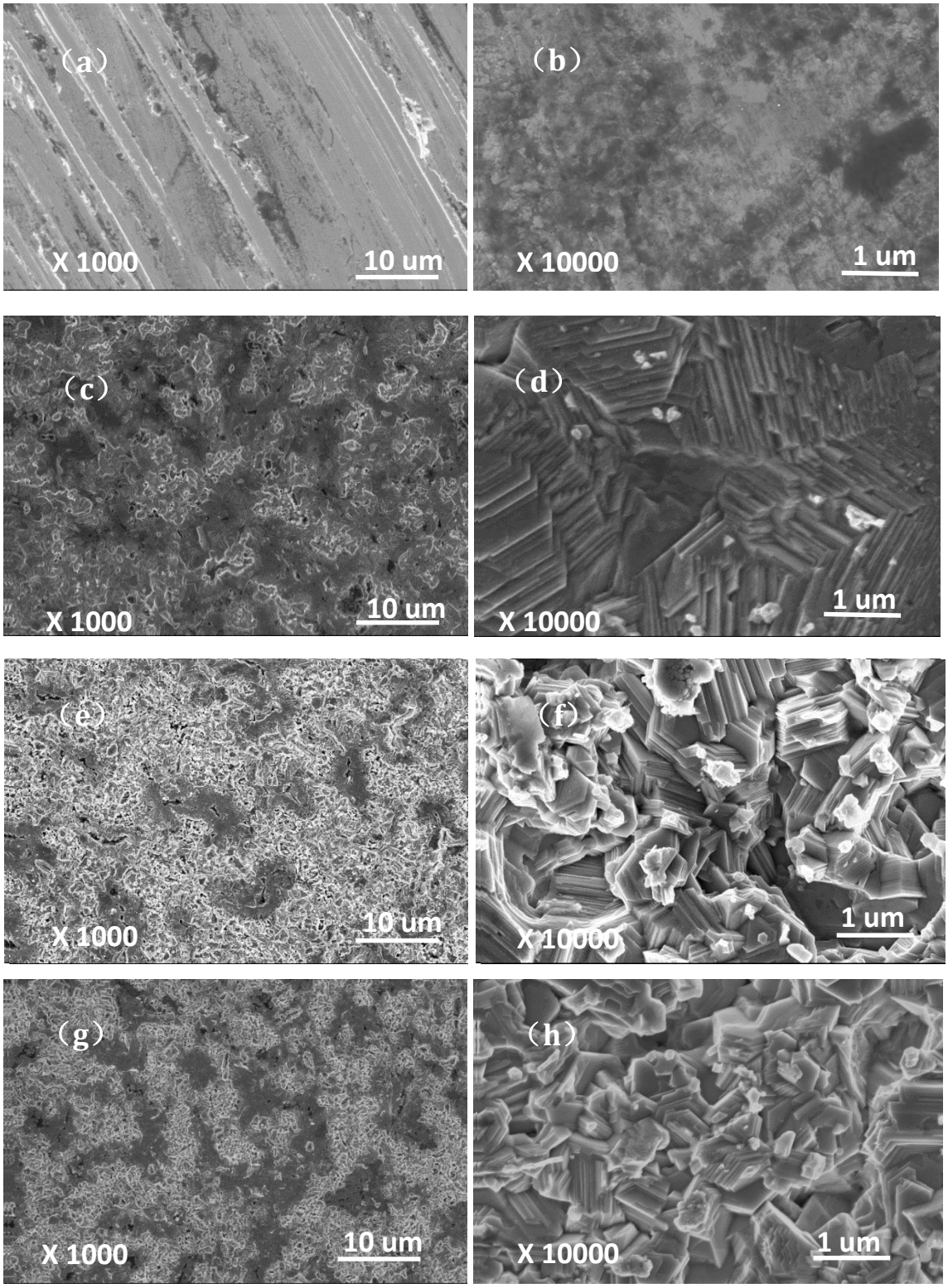

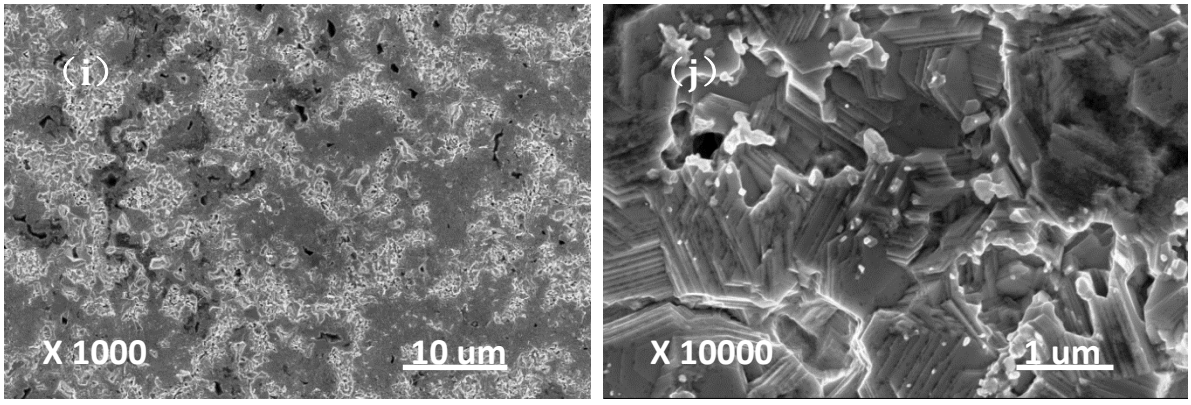

Figure 7.2 SEM image of Zn anodes:

(a) Commercial Zn at X1000 magnification; (b) Commercial Zn at X10000 magnification;

(c) BG#1 at X1000 magnification; (d) BG#1 at X10000 magnification

(e) TG#1 at X1000 magnification; (f) TG#1 at X10000 magnification;

(g) ITG#1 at X1000 magnification; (h) ITG#1 at X10000 magnification;

(i) hBITG#1 at X1000 magnification; (j) hBITG#1 at X10000 magnification;

7.1.2 Corrosion Test by Using Linear Polarization

All anodes had similar corrosion potential and TG#1 had the lowest corrosion current at 723.824 μA (per unit area), follow by ITG#1, commercial Zn, BG#1 and hBITG#1. It means that the anode TG#1 had the best corrosion resistance. Fig. 7.3 shows the Tafel plot result Zn anodes, while Tab. 7.1 gives accurate parameter values.

Table 7.1 Comparison of Tafel fit results on Zn anodes

	E_{corr}	I_{corr}	β_c	β_a
Commercial Zn	-1 436.570 mV	1 360.753 uA	180.2 mV	296.8 mV
BG#1	-1 430.073 mV	4 863.440 uA	227.0 mV	249.9 mV
TG#1	-1 429.395 mV	723.824 μA	163.0 mV	249.9 mV
ITG#1	-1 432.203 mV	937.592 μA	220.5 mV	295.0 mV
hBITG#1	-1 427.145 mV	9 052.225 μA	204.8 mV	180.3 mV

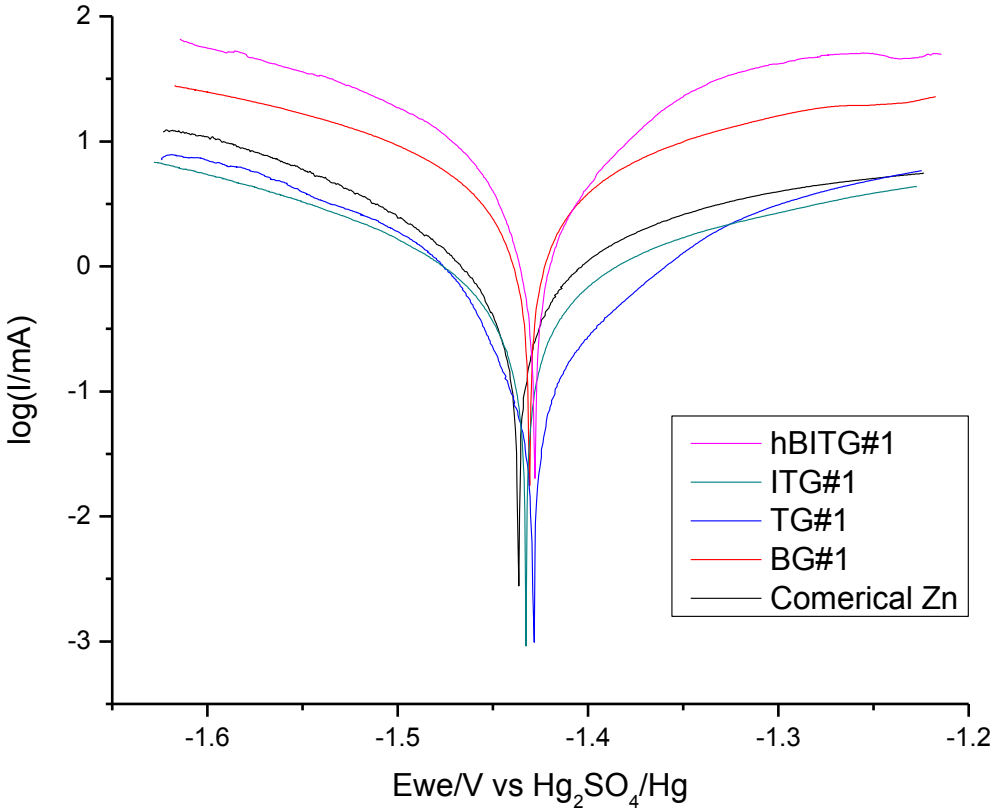

Figure 7.3 Tafel plot result of Zn anodes

7.1.3 Battery Cycle Performance and Electrochemical Impedance Spectroscopy (EIS)

As shown in Figure 7.4 and Table 7.2, After 200 cycles, batteries using commercial Zn anodes had capacity retention of 78.2%, yet batteries with BG#1, TG#1, ITG#1 and hBITG#1 anodes had 82.6%, 84.3%, 75.0%, and 71.9% capacity retention, respectively. While after 300 cycles running, batteries with BG#1, TG#1, ITG#1 and hBITG#1 anodes had 73.2%, 77.2%, 66.2%, and 59.8% capacity retention respectively, yet batteries using commercial Zn anodes were all dead between 220-270 cycles. The results indicate that the TG#1 is the best anode material on battery cycle and all electrowinning Zn anodes are relatively stable compare to commercial Zn.

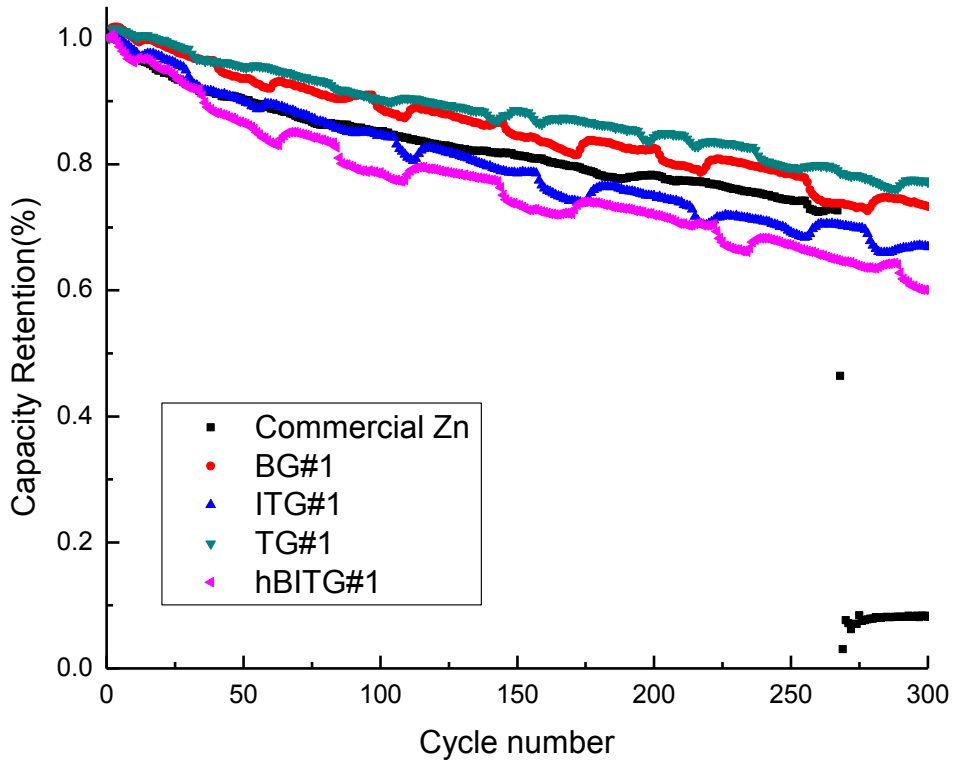

Figure 7.4 Galvanostatic charge/discharge cycle performance of ReHAB system with different Zn anodes.

Table 7.2 Comparison of capacity retention on Zn anodes

	200 cycles	**300 cycles**
Commercial Zn	78.2%	DEAD
BG#1	82.6%	73.2%
TG#1	84.3%	77.2%
ITG#1	75.0%	66.9%
hBITG#1	71.9%	51.8%

Fig. 6.5 displays the Nyquist plots of the EIS measurement for batteries using commercial Zn and hBITG#1 as anode after cycles. The polarization resistances measured by EIS for all kinds of Zn anodes had the same trend compare to their cycle

performance except TG#1 and ITG#1, which indicated thiourea might have some unclear effect on electrowinning Zn anode. The battery with BG#1 anode had smallest polarization resistance which means it consumes the minimum energy during charge-discharge process, followed by hBITG#1, commercial Zn, ITG#1 and TG#1.

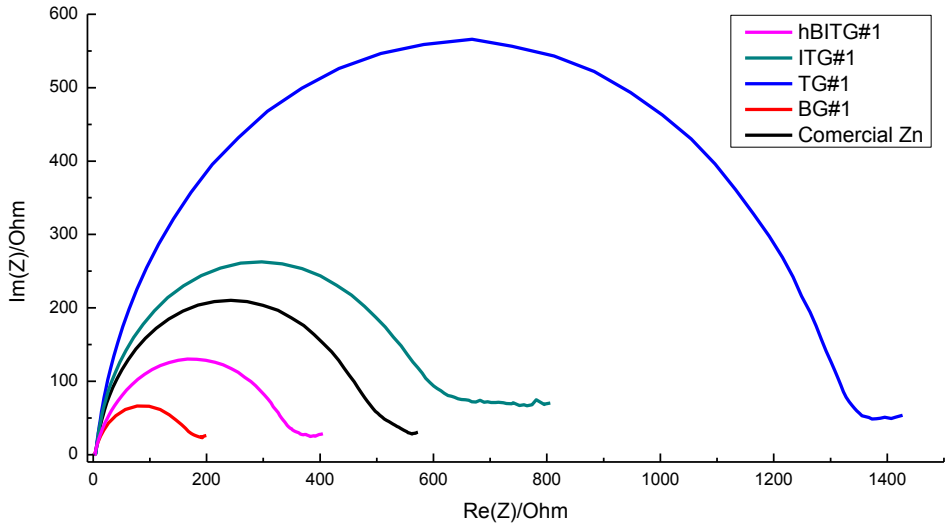

Figure 7.5 EIS profile of ReHAB anodes after 200 cycle test

7.1.4 Float Charge Current

Fig. 7.6 and 7.7 show float charge current and carbon percentages of cathode materials after both room temperature and high temperature float charge. At room temperature (25 ℃), float charge current of commercial Zn and hBITG#1 had largest value means more side reactions happened on batteries, followed by TG#1, BG#1 and ITG#1. While at high temperature (60 ℃), the trend is the same. Results of elemental analysis indicated that batteries with BG#1 anode had the most carbon on cathode material after both RTFC and HTFC which suggests those with BG#1 anode are most stable on cathode material during float charge process, followed by hBITG#1, TG#1, ITG#1 and commercial Zn.

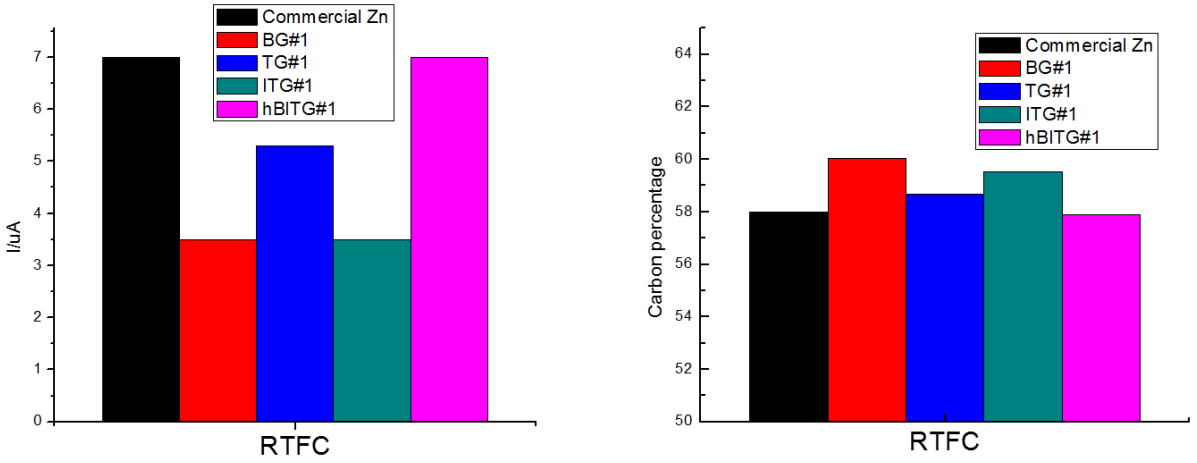

Figure 7.6 Float charge current and carbon percentage of cathode material after float charge at room temperature (RTFC) for Zn anodes

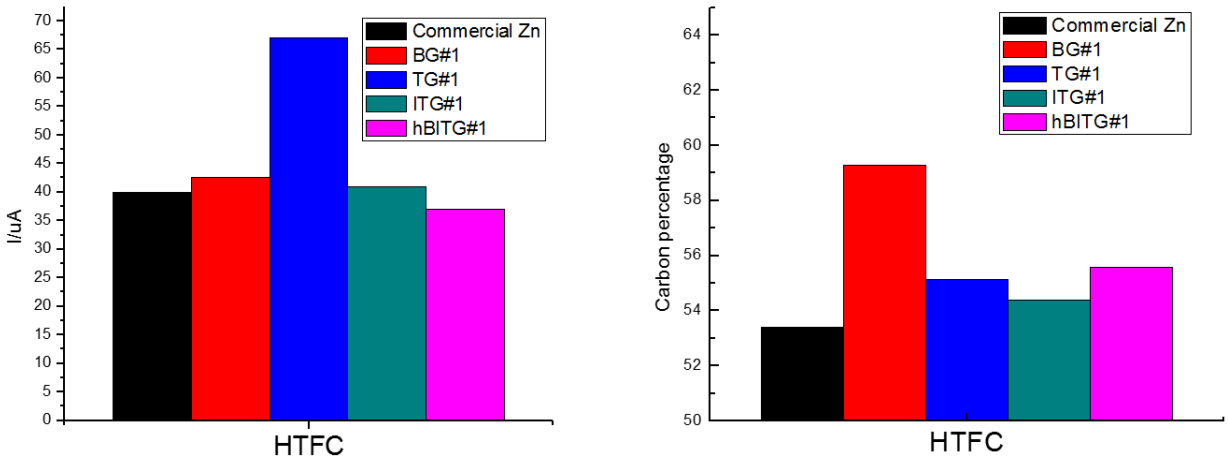

Figure 7.7 Float charge current and carbon percentage of cathode material after float charge at high temperature (HTFC) for Zn anodes

7.1.5 Summary

In summary, both BG#1 and TG#1 anodes show good overall performance. The advantages on battery performance of BG#1 anodes could be attributed to the uniform deposits, preferable crystal orientations and high corrosion resistance. The relative flat surface could inhibit Zn dendrite formation during battery cycle test and could also provide uniform current distribution which is important on float charge process.

The advantages on battery performance of TG#1 anodes could be attributed to the porous and fine-grained deposits, preferable crystal orientations and high corrosion resistance. The porous surface could highly inhibit Zn passivation process by increasing surface area (active material) during battery cycle test. The fine-grained deposits provide relatively uniform current distribution that could contribute to lower float charge current.

It suggests that there are two mechanisms could improve the overall battery performance by modification of Zn anodes. One is inhibit Zn dendrite formation by creating a relative flat surface, while the other is inhibit Zn passivation process by increase surface area. Considering dendrite formation and Zn passivation are the two most important factors in Zn batteries, the results are quite reasonable.

7.1.6 Research significance and novelty

The research has mainly focused on producing different types of electrowinning Zn to apply on ReHAB battery. It is the first time to introduce the electrowinning Zn technology to battery research.

It also provides a possibility for not only ReHAB battery but all kinds of Zn related battery: by modification on Zn anodes, which is electrowinning in our research, some certain kinds of properties could be obtained to improve the performance of the battery. Researchers could adjust Zn anodes to meet the requirement of different uses of batteries, such as UPS.

7.2 Recommendations

More additives with different concentration could be done in order to fully investigate on what kind of electrowinning Zn is best for ReHAB system.

Deep analyze on XRD data (for example, XRD refinement) and impedance data (for example, fitting equivalent circuit) need to be done to make the research more systematic.

The mechanism of how anodes with thiourea as electrowinning additive had opposite results on battery cycle and impedance results should be deeply analyzed by further research.

References

[1] D.Linden, T.B. Reddy, Battery Power and Products Technology, 5 (2008) 10-12.

[2] M. Winter, R.J. Brodd, Chemical Reviews, 104 (2004) 4245-4270.

[3] T. B. Reddy, Handbook of Batteries, 4th Edition, McGraw-Hill, 2011.

[4] B. Schumm, Retrieved from http://www.britannica.com/EBchecked/topic/56126/battery/45858/Development-of-batteries, (2014).

[5] M. Yoshio, R.J. Brodd, A. Kozawa, Lithium-Ion Batteries, Springer, 2009.

[6] A.R. Armstrong, P.G. Bruce, Nature, 381 (1996) 499-500.

[7] C.J. Orendorff, D. Doughty, E.P. Roth, J.A. Jeevarajan, C.S. Winchester, R. Spotnitz, R. Muller, Interface-Electrochemical Society, 21 (2012) 35.

[8] J.-M. Tarascon, M. Armand, Nature, 414 (2001) 359-367.

[9] W. Li, J. Dahn, D. Wainwright, Science, 264 (1994) 1115-1118.

[10] G. Wang, L. Fu, N. Zhao, L. Yang, Y. Wu, H. Wu, Angewandte Chemie, 119 (2007) 299-301.

[11] G. Wang, S. Zhong, D. Bradhurst, S. Dou, H. Liu, Journal of Power Sources, 74 (1998) 198-201.

[12] G. Wang, N. Zhao, L. Yang, Y. Wu, H. Wu, R. Holze, Electrochimica Acta, 52 (2007) 4911-4915.

[13] J. Yan, J. Wang, H. Liu, Z. Bakenov, D. Gosselink, P. Chen, Journal of Power Sources, 216 (2012) 222-226.

[14] M. Thackeray, W. David, P. Bruce, J. Goodenough, Materials Research Bulletin, 18 (1983) 461-472.

[15] M. Thackeray, P. Johnson, L. De Picciotto, P. Bruce, J. Goodenough, Materials Research Bulletin, 19 (1984) 179-187.

[16] K. Cathro, K. Cedzynska, D. Constable, P. Hoobin, Journal of Power Sources, 18 (1986) 349-370.

[17] E. Hosono, T. Kudo, I. Honma, H. Matsuda, H. Zhou, Nano Letters, 9 (2009) 1045-1051.

[18] Y. Yuan, H. Wu, S. Guo, J. Wu, J. Yang, X. Wang, J. Tu, Applied Surface Science, 255 (2008) 2225-2229.

[19] Q. Feng, H. Kanoh, Y. Miyai, K. Ooi, Chemistry of Materials, 7 (1995) 1226-1232.

[20] K. Amine, J. Liu, S. Kang, I. Belharouak, Y. Hyung, D. Vissers, G. Henriksen, Journal of Power Sources, 129 (2004) 14-19.

[21] S.-H. Kang, J.B. Goodenough, L.K. Rabenberg, Chemistry of Materials, 13 (2001) 1758-1764.

[22] M.S. Hong, S.H. Lee, S.W. Kim, Electrochemical and Solid-State Letters, 5 (2002) A227-A230.

[23] M.S. Moats, J.B. Hiskey, D.W. Collins, Hydrometallurgy, 56(2000) 255-268.

[24] M.K. Jha, V. Kumar, R. Singh, Resources, Conservation and Recycling, 33 (2001) 1-22.

[25] V. Ettel, B. Tilak, Electrolytic refining and winning of metals, Comprehensive Treatise of Electrochemistry, Springer, 1981, pp. 327-380.

[26] F. Habashi, Principles of extractive metallurgy, CRC Press, 1969.

[27] M.C. Fuerstenau, K.N. Han, Principles of Mineral Processing, SME, 2003.

[28] A. Scott, R. Pitblado, G. Barton, Proceedings of the Twentieth International Symposium on the Application of Computers and Mathematics in the Mineral Industries, Metallurgy, 1987, pp. 51-62.

[29] A. Scott, R. Pitblado, G. Barton, A. Ault, Journal of Applied Electrochemistry, 18 (1988) 120-127.

[30] J. J. Henderson, H. L. Montague, US Patent 2863810, 1958.

[31] J.M.B. D.J. Machinnon, P.L. Fenn, Journal of Applied Electrochemistry, 17 (1987) 1129-1143.

[32] B. Tripathy, S. Das, G. Hefter, P. Singh, Journal of Applied Electrochemistry, 27 (1997) 673-678.

[33] G.M. Liana Muresan, L. Oniciu, Delia Gaga, Hydrometallurgy, 43 (1996) 345-354.

[34] B. Tripathy, S. Das, P. Singh, G. Hefter, V. Misra, Journal of Electroanalytical Chemistry, 565 (2004) 49-56.
[35] B. Tripathy, S. Das, G. Hefter, P. Singh, Journal of Applied Electrochemistry, 28 (1998) 915-920.
[36] B. Thomas, D. Fray, Journal of Applied Electrochemistry, 11 (1981) 677-683.
[37] R. Kerby, H. Jackson, T. O'keefe, Y.-M. Wang, Metallurgical Transactions B, 8 (1977) 661-668.
[38] M. Karavasteva, S. Karaivanov, Journal of Applied Electrochemistry, 23 (1993) 763-765.
[39] D.R. Fosnacht, T.J. O'Keefe, Metallurgical Transactions B, 14 (1983) 645-655.
[40] D. Mackinnon, R. Morrison, J. Brannen, Journal of Applied Electrochemistry, 16 (1986) 53-61.
[41] D. Mackinnon, P. Fenn, Journal of Applied Electrochemistry, 14 (1984) 467-474.
[42] A.L. Mular, D.N. Halbe, D.J. Barratt, Mineral Processing Plant Design, Practice, and Control, Society for Mining Metallurgy, 2002.
[43] A.E.E. A.E. Saba, Hydrometallurgy, 54 (2000) 91-106.
[44] H.G. Jianming Lu, David Dreisinger, Bruce Downing, Journal of Metallurgical Engineering(ME), 2 (2013) 79-87.
[45] W. Juda, R.J. Allen, A. Bar-Ilan, US Patent 4412894, 1983.
[46] R. Moskalyk, A. Alfantazi, A.S. Tombalakian, D. Valic, Minerals Engineering, 12 (1999) 65-73.
[47] A. Ault, E. Frazer, Journal of Applied Electrochemistry, 18 (1988) 583-589.
[48] C. Cachet, R. Wiart, I. Ivanov, S. Rashkov, Journal of Applied Electrochemistry, 23 (1993) 1011-1016.
[49] C. Bozhkov, M. Petrova, Journal of Applied Electrochemistry, 22 (1992) 73-81.
[50] D. Fosnacht, T. O'keefe, Journal of Applied Electrochemistry, 10 (1980) 495-504.
[51] D. Robinson, T. O'keefe, Journal of Applied Electrochemistry, 6 (1976) 1-7.
[52] D. De Biasio, C. Krauus, Canadian Patent 978137, 1971.
[53] B. Tripathy, S. Das, P. Singh, G. Hefter, Journal of Applied Electrochemistry, 29 (1999) 1229-1235.
[54] S. Das, P. Singh, G. Hefter, Journal of Applied Electrochemistry, 27 (1997) 738-744.
[55] D. MacKinnon, J. Brannen, R. Morrison, Journal of Applied Electrochemistry, 18 (1988) 252-256.
[56] L. Mureşan, G. Maurin, L. Oniciu, S. Avram, Hydrometallurgy, 40 (1996) 335-342.
[57] T. Biegler, E. Frazer, Journal of Applied Electrochemistry, 16 (1986) 654-662.
[58] D. McMullan, Scanning, 17(1995) 175-185.
[59] M.F.C. Ladd, R.A. Palmer, Structure Determination by X-ray Crystallography, Springer, 1985.
[60] Y. Liu, P. Liu, Publishing House of Chemical Industry, (2003) 202.
[61] R. Kuzel, V. Valvoda, M. Chladek, J. Musil, J. Matous, Thin Solid Films, 263 (1995) 150-158.
[62] W.-j. HUANG, J. Vincent, Transactions of Nonferrous Metals Society of China, 16 (2006) s735-s738.
[63] L. Muresan, L. Oniciu, M. Froment, G. Maurin, Electrochimica Acta, 37 (1992) 2249-2254.
[64] M.G. Fontana, Corrosion Engineering, Tata McGraw-Hill Education, 2005.
[65] M. Stern, A.L. Geary, Journal of the Electrochemical Society, 104 (1957) 56-63.
[66] G.F. Ortiz, I. Hanzu, P. Lavela, J.L. Tirado, P. Knauth, T. Djenizian, Journal of Materials Chemistry, 20 (2010) 4041-4046.
[67] W. Zhang, M. Li, Q. Wang, G. Chen, M. Kong, Z. Yang, S. Mann, Advanced Functional Materials, 21 (2011) 3516-3523.
[68] M.E. Orazem, B. Tribollet, Electrochemical Impedance Spectroscopy, John Wiley & Sons, 2011.
[69] J.R. Macdonald, E. Barsoukov, History, 1 (2005) 8.
[70] W.D. Reeve, DC Power System Design for Telecommunications, John Wiley & Sons, 2006.
[71] B. Moeller, J. Moeller, RV Electrical Systems: A Basic Guide to Troubleshooting, Repairing and Improvement, McGraw Hill Professional, 1994.
[72] J.M. McAndrews, R.H. Jones, Telecommunications Energy Conference, 1996. INTELEC'96., 18th

International, IEEE, 1996, pp. 507-513.
[73] A.F. Creaco, E.A. Kussmaul, US Patent 5311112, 1994.
[74] T. Suntio, A. Glad, P. Waltari, Telecommunications Energy Conference, 1996. INTELEC'96., 18th International, IEEE, 1996, pp. 227-233.
[75] J.K. Klang, US Patent 5583416, 1996.
[76] D.J. Theobald, US Patent 5510693, 1996.
[77] P. Adcock, A. Ault, O. Newman, Journal of Applied Electrochemistry, 15 (1985) 865-878.
[78] F. Mansfeld, Corrosion, 29 (1973) 397-402.
[79] M. McKubre, D. Macdonald, Journal of the Electrochemical Society, 128 (1981) 524-530.
[80] S. Müller, F. Holzer, O. Haas, Journal of Applied Electrochemistry, 28 (1998) 895-898.
[81] H. Yang, Y. Cao, X. Ai, L. Xiao, Journal of Power Sources, 128 (2004) 97-101.